

**Preparation of N-Doped Carbon Quantum Dots and Their  
Applications in the Selective Sensing of Mercury (II)**

by © Xiangyu Yan submitted  
to the School of Graduate Studies in partial fulfillment  
of the requirements for the degree of

Master of Engineering  
Faculty of Engineering and Applied Science  
Memorial University of Newfoundland

February, 2021

St. John's Newfoundland and Labrador

## Abstract

This master's thesis presents a comprehensive study on the optimal design and synthesis of nitrogen-doped carbon quantum dots (N-CQDs) from small molecule carbon and nitrogen precursors and their application as fluorescence sensor for the detection of heavy metal ions. By employing the Box-Behnken design (BBD), the optimal synthetic condition for hydrothermal method was obtained, which led to the achievement of the high quantum yield of 51.7% for N-CQDs. The as-prepared N-CQDs are with brownish-yellow color and showed a bright blue light irradiation. To stabilize the N-CQDs, immobilization of N-CQDs onto a glutaraldehyde cross-linked chitosan was then performed to prepare the N-CQDs@GACTS hydrogel film for the selective sensing of  $\text{Hg}^{2+}$  ion. FTIR and XPS analyses revealed that N-CQDs were embedded into the GACTS matrix mainly through weak hydrogen bond or electrostatic attraction. Among the three tested heavy metal ions ( $\text{Cd}^{2+}$ ,  $\text{Hg}^{2+}$  and  $\text{Pb}^{2+}$ ), the N-CQDs@GACTS hydrogel film exhibited remarkable sensing sensitivity and selectivity of  $\text{Hg}^{2+}$ . The excellent selectivity could be attributed to a stronger interaction between the hydrogel film and  $\text{Hg}^{2+}$  ion. Due to the strong oxidizing ability and chelating power,  $\text{Hg}^{2+}$  can be more readily combined with polar groups on the surface of N-CQDs@GACTS hydrogel to form new complexes by either chelation or electrostatic attraction, which provokes an effective electron transfer for the fluorescence quenching of the N-CQDs@GACTS hydrogel. The prepared N-CQDs@GACTS hydrogel demonstrates enhanced practicality in terms of fast response, sensitivity, selectivity, and economical pricing. It has great potential for practical applications in selectively detecting  $\text{Hg}^{2+}$  from either drinking water or wastewater.

## **Acknowledgments**

First and foremost, I would like to express my sincere gratitude to my supervisors Dr. Yan Zhang and Dr. Faisal Khan for their motivation and continuous support during my Master's study. Special thanks to Dr. Yan Zhang for unreservedly passing on to me her knowledge and skills required to carry out the research work and present the research outcomes.

I am very grateful to Memorial University and the Natural Sciences and Engineering Research Council of Canada (NSERC) for financial support during my study.

I am extending my thanks to Dr. Yuming Zhao and Dr. Zahra A. Tabasi for their help in measuring the fluorescence spectra of CQDs samples and determination of the quantum yields.

I am incredibly grateful to my parents for their love, care, support, and sacrifice for my educating and daily life.

Finally, my thanks go to all the people who have supported me to complete the research work directly or indirectly.

## Table of Contents

<b>ABSTRACT</b> .....	<b>I</b>
<b>ACKNOWLEDGMENTS</b> .....	<b>II</b>
<b>TABLE OF CONTENTS</b> .....	<b>III</b>
<b>LIST OF TABLES</b> .....	<b>VI</b>
<b>LIST OF FIGURES</b> .....	<b>VII</b>
<b>LIST OF ABBREVIATIONS AND SYMBOLS</b> .....	<b>IX</b>
<b>CHAPTER 1 INTRODUCTION</b> .....	<b>1</b>
<b>1.1 BACKGROUND</b> .....	<b>1</b>
<b>1.2 RESEARCH OBJECTIVES</b> .....	<b>4</b>
<b>1.3 STRUCTURE OF THE THESIS</b> .....	<b>5</b>
<b>CHAPTER 2 LITERATURE REVIEW</b> .....	<b>6</b>
<b>2.1 PREPARATION METHODS FOR CQDS</b> .....	<b>6</b>
<b>2.1.1 Top-down methods</b> .....	<b>6</b>
<b>2.1.2 Bottom-top methods</b> .....	<b>8</b>
<b>2.1.3 Heteroatom doping</b> .....	<b>11</b>
<b>2.1.4 Surface passivation</b> .....	<b>15</b>
<b>2.2 CQD-BASED COMPOSITE MATERIALS</b> .....	<b>16</b>
<b>2.2.1 CQD-incorporated polymeric hydrogels</b> .....	<b>16</b>
<b>2.2.2 CQD- loaded polymeric films</b> .....	<b>17</b>
<b>2.2.3 CQD-loaded metallic semiconductors</b> .....	<b>19</b>
<b>2.3 CHARACTERIZATION OF CQDS AND CQD-BASED COMPOSITE MATERIALS</b> .....	<b>20</b>
<b>2.3.1 FTIR</b> .....	<b>20</b>
<b>2.3.2 TEM</b> .....	<b>22</b>
<b>2.3.3 UV/Vis spectroscopy</b> .....	<b>22</b>
<b>2.3.4 Fluorescence spectroscopy</b> .....	<b>24</b>
<b>2.3.5 XPS</b> .....	<b>25</b>

2.4 APPLICATIONS OF CQD-BASED FUNCTIONAL MATERIALS .....	26
2.4.1 Bioimaging .....	26
2.4.2 Sensing.....	28
2.4.3 Photocatalysis .....	30
<b>CHAPTER 3 ONE-POT SYNTHESIS OF N-DOPED CQDS .....</b>	<b>32</b>
3.1 INTRODUCTION.....	32
3.2 MATERIALS AND METHODS .....	34
3.2.1 Materials .....	34
3.2.2 The Preparation of N-CQDs.....	35
3.2.3 Design of experiments (DOE) for the preparation of N-CQDs.....	35
3.2.4 Analytical methods.....	36
3.2.5 Determination of quantum yield (QY).....	37
3.3 RESULTS AND DISCUSSION .....	37
3.3.1 DOE optimization of synthetic conditions.....	37
3.3.2 Characterization of the as prepared N-CQDs.....	44
3.3.3 Optical properties of N-CQDs.....	48
3.4 CONCLUSION .....	51
<b>CHAPTER 4 CQDS-INCORPORATED CHITOSAN HYDROGEL FILM FOR SELECTIVE SENSING OF Hg<sup>2+</sup> ION.....</b>	<b>52</b>
4.1 INTRODUCTION.....	52
4.2 MATERIALS AND METHODS .....	55
4.2.1 Materials .....	55
4.2.2 Synthesis of fluorescent N-CQDs .....	55
4.2.3 Preparation of N-CQDs@GACTS hydrogel film .....	56
4.2.4 Selective sensing of Hg <sup>2+</sup> ion .....	56
4.2.5 Characterization.....	57
4.3 RESULTS AND DISCUSSION .....	57
4.3.1 Degree of crosslinking for GACTS hydrogel films .....	57

4.3.2 Characterization of N-CQDs@CTS hydrogel film.....	58
4.3.3 Optical properties of N-CQDs@GACTS film.....	60
4.3.4 Sensing selectivity of N-CQDs@GACTS hydrogel.....	61
4.3.5 Sensing of Hg <sup>2+</sup> ions .....	63
4.3.6 Sensing mechanism.....	65
4.4 CONCLUSION .....	67
<b>CHAPTER 5 CONCLUSION AND RECOMMENDATION.....</b>	<b>69</b>
5.1 SUMMARY .....	69
5.2 RECOMMENDATIONS FOR FUTURE WORK .....	70
<b>REFERENCES.....</b>	<b>72</b>

## List of Tables

Table 2.1	The comparison of top-down and bottom-up synthetic methods of CQDs .....	10
Table 2.2	Summary of the preparation methods and properties of heteroatom-doped CQDs .....	13
Table 2.3	Metal ion sensing by chemical-derived CQDs .....	29
Table 3.1	Box-Behnken design .....	36
Table 3.2	Reaction conditions for hydrothermal preparation of N-CQDs.....	38
Table 3.3	The ANOVA results for the model .....	41
Table 4.1	Comparison of detection performances of CQDS-based composites for Hg <sup>2+</sup> .....	63

## List of Figures

Figure 3.1	The 3D surface under different ratio of EDA:CA.....	43
Figure 3.2	TEM image of N-CQDs.....	44
Figure 3.3	XPS survey spectrum of N-CQDs .....	44
Figure 3.4	High resolution C 1s (a); N 1s (b); and O 1s (c) XPS spectra of N-CQDs .....	45
Figure 3.5	FTIR spectra of CA and N-CQDs.....	47
Figure 3.6	The UV-Vis absorption and fluorescence spectra of N-CQDs ( $\lambda_{ex} = 350$ nm).....	48
Figure 3.7	Emission spectra of N-CQDs under different excitation wavelengths ...	49
Figure 3.8	The effect of pH on fluorescence spectra of N-CQDs ( $\lambda_{ex} = 350$ nm) ..	51
Figure 4.1	GACTS hydrogel films with different degrees of crosslinking: 0%(a); 5%(b); 10%(c).....	58
Figure 4.2	FTIR spectra of chitosan, GACTS and N-CQDs@GACTS films.....	59
Figure 4.3	XPS survey spectra of N-CQDs@GACTS film before and after Hg <sup>2+</sup> sensing .....	60
Figure 4.4	The excitation and emission spectra of (a) GACTS film and (b) N-CQDs@GACTS films .....	61
Figure 4.5	The I/I <sub>0</sub> ratio of N-CQDs@GACTS hydrogel in the presence of 100nM different metal ions (a); and images of N-CQDs@GACTS hydrogel in the presence of metal ions under 395nm UV light (b).....	62
Figure 4.6	The fluorescence intensity spectra of N-CQDs@GACTS hydrogel in the presence of Hg <sup>2+</sup> ion (0~100 $\mu$ M) (a); The fluorescence quenching rates of N-CQDs@GACTS hydrogel under different concentrations of Hg <sup>2+</sup> (b); Time-dependent fluorescence intensity of N-CQDs@GACTS hydrogel (c) .....	64
Figure 4.7	High resolution and deconvoluted N 1s (a), O 1s (c) and Hg 4f (e) XPS spectra of N-CQDs@GACTS film before Hg <sup>2+</sup> sensing; N 1s (b), O 1s (d)	



and Hg 4f (f) XPS spectra of N-CQDs@GACTS film after Hg<sup>2+</sup> sensing.  
..... 66

## List of Abbreviations and Symbols

A	The absorbance measured at excited wavelength
A <sub>C</sub>	The absorbance of carbon dots
A <sub>R</sub>	The absorbance of quinine sulfate
Abs	The absorption spectra
BBD	Box-Behnken designs
CA	Citric acid
CQDs	Carbon quantum dots
CTS	Chitosan
DOE	Design of experiment
EDA	Ethylenediamine
E <sub>x</sub>	The excitation spectra
E <sub>m</sub>	The emission spectra
FTIR	Fourier-transform infrared spectroscopy
FL	Fluorescence
GA	Glutaraldehyde
I	The FL intensity in the presence of heavy metal ions
I <sub>0</sub>	The FL intensity in the absence of heavy metal ions
ICP-OES	Inductively coupled plasma optical emission spectroscopy
ICP-MS	Inductively coupled plasma mass spectroscopy
N-CQDs	Nitrogen-doped carbon quantum dots
PL	Photoluminescence

QY	Quantum yield
QY <sub>C</sub>	The quantum yield of N-CQDs
QY <sub>R</sub>	The quantum yield of quinine sulfate
S <sub>c</sub>	The FL intensity of N-CQDs
S <sub>R</sub>	The FL intensity of quinine sulfate
TEM	Transmission electron microscope
UV-vis	Ultraviolet-visible spectroscopy
XPS	X-ray photoelectron spectra
$\eta$	The refractive index of the solvent
$\eta_C$	The refractive index of N-CQDs
$\eta_R$	The refractive index of quinine sulfate
$\lambda_{ex}$	The excitation wavelength

# Chapter 1 Introduction

## 1.1 Background

Quantum dots (QDs) are a kind of quasi-spherical nanoparticles typically ranging from 1 to 10 nm, composed of elements from the periodic groups II–VI (Ciftja, 2012). QDs have unique optical properties, such as good fluorescence stability, wide excitation and emission spectra, which enable them to be exploited in applications of sensing, imaging, solar, and optoelectronic devices. However, conventional QDs are usually made from semiconducting materials, especially cadmium and selenium, in organic-phase or in water-phase system, which has raised concerns over toxicity and high cost (Molaei, 2019). In the last two decades, fluorescent carbon quantum dots (CQDs), primarily composed of carbon with some hydrogen, oxygen and nitrogen moieties, have gained increasing research attention due to their excellent biocompatibility, outstanding optical property, low toxicity and resistance to photobleaching (Gao et al., 2016).

Fluorescence is the process of light emission by a material that absorbs light at a lower wavelength (higher energy) and emits light of longer wavelength (lower energy). Fluorescence stops within a few hundred nanoseconds once the light source is removed. The ratio between the numbers of emitted and absorbed photons is the fluorescence quantum yield (QY), and the average time that a fluorophore remains in its excited state before the emission of photons is its fluorescence lifetime (Li et al., 2019). As thus, development of eco-friendly fluorescent CQDs with high quantum yield and long fluorescence lifetime is highly desirable for many practical applications.

Although various synthetic methods are available to prepare CQDs from different precursors, hydrothermal/solvothermal carbonization has been considered an

inexpensive and environment-friendly method to produce highly fluorescent CQDs in large quantities. However, the ready availability of large quantities of CQDs is often counterbalanced by their poor homogeneity and definability (Kozák et al., 2016). The structure, chemical composition, and surface chemistry of the resulting CQDs can vary substantially. These properties are often not even precisely determined because the difficulty in controlling the reaction rates during their synthesis and CQDs tend to be rather heterogeneous. The heterogeneity of CQDs (e.g., the presence of functionalized surface defects) contributes to their multicolor (excitation wavelength-dependent) emissions that result in low QY of CQDs (Molaei, 2019). New approaches are needed to optimize the reaction conditions and hence to control the degree of crystallinity and functionalization of CQDs for enhanced QY.

Functionalization of CQDs is extremely useful for effectively tuning their intrinsic structure and surface state. Heteroatom doping and surface modification are two functionalization strategies to tune the fluorescent properties of CQDs (Chen et al., 2019). Doping non-metallic elements (such as N, S, B and P) in CQDs does not originate the photoluminescence (PL) directly but it effects the PL behavior to produce tunable optical properties with high QY (Li et al., 2012). Zhang et al. (2012) have tuned the emission of CQDs from blue to yellow through N-doping. They found that new emission centers were formed with the increasing N content, which induced the red shifting of fluorescence spectra. A QY as high as 73% was achieved for N and S co-doped CQDs due to a synergistic effect between the doped nitrogen and sulfur atoms (Dong et al., 2013). Other than heteroatom doping, surface modification can also be applied for altering active sites and the functional groups on the CQDs surface, which can endow fluorescent CQDs with the unique properties resulting from the introduced

functional ligands. Despite the extensive research efforts made on functionalization of CQDs over the past several years, there still lacks the effective methods to precisely identify the chemical structure and composition of CQDs product and hence to elucidate the mechanisms of PL. More theoretical and experimental works or combination of both should be carried out to fully understand the PL mechanism of CQDs.

CQDs have been the subject of intense research related to a multitude of applications such as biomonitoring, drug and gene delivery, sensors, and photocatalysis (Jing et al., 2019). In recent years, the use of CQDs as fluorescence sensors for heavy metal detection has been investigated intensively. Detection of heavy metal ions has been of great interest in light of their huge impacts on the environment and human health. Compared with conventional detection methods (e.g., atomic absorption technique (AAS), inductively coupled plasma-optical emission spectrometry (ICP-OES) and inductively coupled plasma-mass spectrometry (ICP-MS)), CQDs as novel fluorescence sensors exhibit the advantages of intrinsic simplicity, high sensitivity, low cost and simple equipment requirement (Pan et al., 2015). So far, a series of CQDs-based fluorescent sensors for  $\text{Fe}^{3+}$ ,  $\text{Hg}^{2+}$ ,  $\text{Ag}^+$ ,  $\text{Pb}^{2+}$ ,  $\text{Cu}^{2+}$ , and  $\text{Cr}^{6+}$  has been reported (Guo et al., 2017; Lim et al., 2015; Karami et al., 2020; Yang et al., 2016; Yuan et al., 2016). Nonetheless, two big issues were observed from these studies when using CQDs solution directly as fluorescence sensors. The first problem is that bare CQDs tend to aggregate in the solution, which leads to unstable (time-dependent) fluorescence intensity. The second issue is that CQDs are highly hydrophilic and are difficult to remove from metal solutions (analytes), it was thus unable to reuse of the fluorescent CQDs (Liu et al., 2019). As such, preparation of solid-phase CQDs-based nanocomposites may solve the above-mentioned problems.

Immobilization of CQDs onto an appropriate solid matrix is an effective pathway to stabilize CQDs as well as to improve their PL performances (Wang et al., 2016). The solid matrices help control the assembly shape, interparticle distance, size and porosity, and provide versatile advantages of improved mechanical strength, chemical and optical stability for CQDs. Through electrostatic interactions, covalent bonds, non-covalent bonds or hydrogen bonds, CQDs have been incorporated into different solid matrices to prevent aggregation-induced fluorescence quenching and produce fluorescent materials for bioimaging and sensing applications (Kang & Lee, 2019; Wolfbeis 2015). But there are insufficient research studies on the preparation of CQDs-incorporated nanocomposite materials for heavy metal sensing. More research efforts need to be made to develop fast response, sensitive and selective CQDs-based nanocomposites as fluorescence sensors for heavy metal detection.

## **1.2 Research Objectives**

In order to partially solve the aforementioned research gaps, the current study was focused on the development of a novel CQDs-incorporated composite material as fluorescence sensor for the selective sensing of mercury ions.

This study entailed the following tasks: i) preparation of nitrogen-doped CQDs (N-CQDs) from citric acid and ethylenediamine using hydrothermal method; ii) applying design of experiments (DOE) to optimizing the hydrothermal reaction conditions for the maximum QY of N-CQDs; iii) fabrication of N-CQDs-incorporated glutaraldehyde cross-linked chitosan (N-CQDs@GACTS) hydrogel film for heavy metal sensing; and iv) clarification of the selective sensing mechanism of the as-prepared N-CQDs@GACTS hydrogel film to Hg<sup>2+</sup> ion using different characterization methods.

### 1.3 Structure of the Thesis

This thesis includes five chapters. Following this brief introduction, development and the most important applications of CQDs and CQDs-based composite materials are reviewed in Chapter 2. Chapter 3 focuses on the DOE optimization of the synthetic conditions and the characterization of N-CQDs by TEM, FTIR, XPS, UV-vis and FL spectroscopy. Chapter 4 presents the synthesis of the N-CQDs@GACTS hydrogel film, its application on the detection of  $\text{Cd}^{2+}$ ,  $\text{Hg}^{2+}$  and  $\text{Pb}^{2+}$ , as well as the sensitivity, selectivity and response time measurements of N-CQDs@GACTS hydrogel for  $\text{Hg}^{2+}$ . Moreover, discussions on the selective sensing mechanism of N-CQDs@GACTS hydrogel film towards  $\text{Hg}^{2+}$  are also included with the aid of XPS analysis of the hydrogel film. Finally, the major conclusions drawn from this study and recommendations for future works are summarized in Chapter 5.



## Chapter 2 Literature Review

Carbon quantum dots (CQDs), a new family of fluorescence carbon nanomaterials, have attracted increasing attention in recent years by virtue of their outstanding photoluminescence properties, photo-stability, low toxicity, and low cost. CQDs are the most intensively studied carbon nanomaterials since their discovery in 2004 for applications in photocatalysis, electrocatalysis, sensors, bioimaging, and drug delivery (Jing et al., 2019). This chapter is dedicated to an overall review on the preparation of CQDs, fabrication of CQD-based composites as well as the applications of CQD-based functional materials.

### 2.1 Preparation Methods for CQDs

The fabrication of CQDs can be generally classified into “top-down” and “bottom-up” approaches. The former involves cleaving or breaking down of carbonaceous materials via chemical, electrochemical, or physical approaches. The latter is implemented by pyrolysis or carbonization of small organic molecules or by step-wise chemical fusion of small aromatic molecules (Tajik et al., 2020).

#### 2.1.1 Top-down methods

The top-down methods, mainly including arc discharge, laser ablation, electrochemical method, and ultrasonic treatment, involve the chemical or mechanical disruption of non-fluorescent macroscopic carbon materials into the nano-size photoluminescent CQDs. In arc discharge method, a direct-current arc voltage is applied across two graphite electrodes immersed in an inert gas, CQDs are generated from crude carbon nanotube soot. In 2004, CQDS were first discovered by Xu and co-workers (Xu et al., 2004) during the purification of the single-walled carbon nanotubes (SWCNTs) through an

oxidation procedure between nitric acid and the arc-discharged soot. Arora and Sharma (2014) synthesized CQDs in a sealed reactor under extremely high temperature using electric current with the aim of production of high energy plasma. However, CQDs produced by the arc discharge method have low yield, and are difficult to purify (Singh et al., 2018).

Laser ablation is a synthesis method of CQDs by laser irradiation of a carbon target. Sun et al. (2006) prepared CQDs with an average size of 5 nm via laser ablation of a carbon target prepared by the thermal-treatment of a mixture of graphite powder and cement in a flow of argon gas carrying water vapor at 900 °C and 75 kPa, followed by the dispersion in nitric acid solution and passivation with polyethylene glycol (PEG). The obtained CQDs demonstrated strong photoluminescence at excitation wavelength of 400 nm. Hu et al. (2011) used pulsed laser to irradiate graphite flakes dispersed in PEG solution for 4 h with ultrasound sonication, which led to the formation of a homogeneous black suspension. CQDs were obtained from the colorful supernatant after centrifugation. Though simple in operation, the laser ablation method needs more carbon materials for the preparation of CQDs and the size distribution of the obtained CQDs is very broad, resulting in low QY.

CQDs can also be synthesized through electrochemical approach. Yao and co-workers (Yao et al., 2014) reported the synthesis of blue fluorescent CQDs with size of 2~3 nm in pure water using the electrochemical method. The resultant CQDs showed excellent fluorescent property and thermodynamic stability in aqueous solution. In another study, Liu et al. (2016) synthesized CQDs with an average diameter of  $4.0 \pm 0.2$  nm and higher crystallinity through electrochemical oxidation of a graphite electrode in the alkaline alcohols. The big advantage of electrochemical method for synthesizing CQDS is its

ability to regulate particle size, purity, affordability, yield, and PL property of the synthesized CQDs (Tajik et al., 2020).

Moreover, energy of ultrasonic waves can be used to cut macroscopic carbon materials into nanoscale CQDs. Ma et al. (2012) have introduced a simple ultrasonic approach for synthesizing nitrogen-doped CQDs (N-CQDs) with the use of the aqua ammonia and glucose as the precursor. The obtained N-CQDs shows high aqueous dispersibility, high stability, and good PL performance under visible light excitation. Recently, Dang and co-workers (Dang et al., 2016) firstly introduced a facile method for large scale fabrication of CQDs through a one-phase ultrasonic procedure using polyamide resin. CQDs with QY of 28.3% were obtained after passivation with a silane coupling agent KH570.

### **2.1.2 Bottom-top methods**

In the bottom-up synthesis, the precursors act as seeds and grow into CQDs under various reaction conditions, commonly by heating or microwave. The main bottom-up approaches for CQDs-preparation are hydrothermal/solvothermal synthesis, microwave-assisted method, and template method. In hydrothermal/solvothermal synthesis, small organic molecules undergo condensation, polymerization, carbonization and passivation processes to form CQDs in water or organic solvent under high temperature and high pressure. The optical properties of CQDs can be easily controlled by adjusting and selecting reaction temperature, time, solvents and raw materials. In addition, this method helps to get a relatively higher QY compared to other methods. Currently, hydrothermal method is the most widely used method for the synthesis of CQDs due to its non-toxicity, low cost, and simple operation (Namdari et al., 2017; Zhuo et al., 2015).

Microwave irradiation of organic compounds is a fast and cheap technique for synthesizing CQDs (Jaiswal et al., 2012; Zhai et al., 2012; Prasad et al., 2013). CQDs can be readily obtained within a few minutes and in improved yield. Wang et al. (2014) presented a facile one-step microwave assisted synthesis of water-soluble phosphorus containing CQDs. A suspension was obtained by heating the phytic acid and ethylenediamine water solution for 8 min in a 750 W microwave oven. The CQDs with two-peak emissions were synthesized. Recently, Pan et al. (2015) successfully prepared the excitation-dependent CQDs from citric acid molecules using microwave assisted method. By adjusting the reaction time and temperature, excitation-dependent (also called full-color) CQDs, which exhibit unusually comparable emission intensity across the entire visible spectrum as shifting the excitation wavelength, were obtained. Although microwave-assisted synthesis may help to get CQDs with more uniform chemical and optical properties, this method is usually restricted to small volumes, limiting their application in large scale reactions (Medeiros et al., 2019). Besides, the pressure of the system is also limited, reducing the usability of solvents with lower boiling points.

Template method for the synthesis of CQDs mainly involves two steps: i) calcination synthesis in the suitable mesoporous template or silicon spheres; and ii) etching to remove supports and generate the nanosized CQDs. Liu et al., (2009) presented a soft–hard template approach toward photoluminescent CQDs with uniform morphologies using the copolymer Pluronic P123 as a soft template and ordered mesoporous silica (OMS) SBA-15 as a hard template. In their study, organic molecules with different aromatic frame-works such as 1,3,5-trimethylbenzene (TMB), diamine benzene (DAB), pyrene (PY) and phenanthroline (PHA), were used as carbon precursor for CQDs with

tunable sizes, compositions and crystallinity. Lai et al. (2012) also reported the growth of CQDs inside the mesoporous silica nanoparticles which acted as a nanoreactor to regulate the size distribution of CQDs. The mixture of mesoporous SiO<sub>2</sub>, glycerol and PEG-NH<sub>2</sub> were heated at 230 °C for 30 min, followed by centrifugation to obtain the CQDs. The resulting CQDs showed enhancement in QY, good colloidal stability and biocompatibility. However, it has to be addressed that template method is costly and time-consuming compared with other methods (Zuo et al., 2016).

Nowadays, many successful examples for bottom-up and top-down synthesis of CQDs can be found in the open literature (Guan et al., 2014; Qu et al., 2014; Hu et al., 2019; Du et al., 2019; Yue et al., 2019; Liu et al., 2019). Compared with top-down strategy, the bottom-up strategy has obvious advantages in selecting various organic precursors and precisely controlling morphology and size distribution, it is therefore more intensively employed for the preparation of CQDs. The main advantages and disadvantages of both synthetic strategies were summarized in Table 2.1.

Table 2.1 The comparison of top-down and bottom-up synthetic methods of CQDs

	<b>Methods</b>	<b>Advantages</b>	<b>Disadvantages</b>
Top-down methods	Arc discharge	High density	Complicated method
	Laser ablation	Stable optical property	Low quantum yield
	Electrochemical		Costly starting materials
	Ultrasound		
Bottom-up methods	Hydro-/solvothermal	Simple method	Single emission wavelength
	Microwave	High quantum yield	
	Template	Cheap raw materials	

### 2.1.3 Heteroatom doping

Among the excellent features, fluorescent property of CQDs is one of the most exciting for researchers in materials and biological science. As a potential fluorescent probe for long- or real-time bioimaging, it is essential to make further efforts to improve the fluorescent properties of CQDs. Heteroatom doping is one of the most convenient and effective way to enhance the fluorescent properties of CQDs. By doping CQDs with heteroatoms, not only the PL intensity, but also the QY of CQDs can be improved.

Various heteroatoms, particularly the non-metals such as nitrogen (N), phosphorus (P), sulfur (S) and boron (B) have been used to dope CQDs. Nitrogen is a typical dopant because it has a comparable atomic size and five valence electrons for bonding with carbon atoms. Li et al., (2012) first use electrochemical method to synthesize N-doped CQDs. It is showed an excellent optoelectronic feature by using nitrogen-containing tetrabutylammonium perchlorate in acetonitrile as the electrolyte to add nitrogen atoms in the CQDs. Liu et al., (2013) reported a one-step solvothermal synthesis of N-doped CQDs as efficient two-photon fluorescent probes using graphene oxide as carbon precursor and dimethylamine as a source of nitrogen. The two-photon-induced fluorescence of CQDs was systematically investigated using near-infrared laser as excitation and applied for efficient two-photon cellular and deep-tissue imaging. Typically, the N-CQDs demonstrate clear blue or green fluorescence.

Compared to N-CQDs, sulfur-doped CQDs (S-CQDs) are relatively difficult to synthesize because C–S bonds are difficult to form. Chandra et al., (2013) firstly developed a facile synthetic route for S-CQDs, which exhibited a wide band gap of 4.43 eV with a high open circuit voltage of 617 mV. The obtained S-CQDs demonstrated good water dispersibility, high photostability, negligible toxicity and bright blue

fluorescence, rendering the great potential as an excellent bioimaging agent and/or drug delivery carrier. Xu et al., (2014) prepared the S-doped CQDs via the hydrothermal method and get a highest QY of 67% by using sodium citrate and sodium thiosulfate as precursors. Ge et al., (2015) prepared the first red-emissive S-doped CQDs by hydrothermal treatment of polythiophene phenylpropionic acid. The resulting S-CQDs showed broad light absorption, high photothermal conversion efficiency, and visible light excitation.

Co-doping of multiple heteroatoms becomes an available method to further enhance the PL intensity of CQDs. Co-doping allows the formation of well-distributed surface states and a reduction in non-radiative recombination, resulting in an increase of QY of the synthesized CQDs. Kim et al., (2018) demonstrated that B and N co-doped CQDs (BN-CQDs) with an 80 % QY compared to N-CQDs with a 40 % QY. With thorough structural analyses, BN-CQDs were found to consist of graphitic N and well-distributed surface states including hydroxyl and carbonyl groups. The unique structure of BN-CQDs influenced the dynamics of charge recombination, thus leading to high QY in both the solution state (80 %) and the solid state (67.7 %). Dong and co-workers (Dong et al., 2013) reported N and S co-doped CQDs by using l-cysteine and citric acid as N, S and C sources. The synthesized CQDs showed a high QY of 73% and excitation-independent emission stemmed from the enhancement of the N defect states by means of S co-doping.

Table 2.2 summarizes the preparation methods and properties of heteroatom-doped CQDs reported in the open literature.

Table 2.2 Summary of the preparation methods and properties of heteroatom-doped CQDs

Heteroatoms	Precursors	Synthetic methods	Particle size, nm	Ex/Em, nm	QY, %	Ref.
N	Carbon tetrachloride and Sodium amide	Solvothermal synthesis	2.5	365/432	22	Zhang et al., 2012
N	Citric acid, formamide	Solvothermal synthesis	6.8	540/637	26.2	Pan et al., 2015
N	citric acid and ethylenediamine	Soft-template	2.0	360/438	25-87	Do et al., 2014
N	1,2-ethylenediamine, 1,3-propanediamine, and 1,4-butanediamine	Solvothermal	3.0	317/390	20.4-36.3	Qian et al., 2014
N	Carbon nanoparticles and DMF	Acid exfoliation and hydrothermal	3-8	324/428	39	Yang et al., 2014
S	Poly(sodium 4-styrene sulfonate)	Hydrothermal	5	370/430	9	Travlou et al., 2017
S	Sodium citrate and sodium thiosulfate	Hydrothermal	4.6	350/440	67	Xu et al., 2015
S	graphite rod and sodium <i>p</i> -toluenesulfonate	Electrolysis	3	380/480	10.6	Li et al., 2014
S	Thiomalic acid	Sulfuric acid treatment	2	340/446	11.8	Chandra et al., 2013
P	Phosphorous tribromide and hydroquinone	Solvothermal	3-5	372/440	25	Zhou et al., 2014
P	phosphorus-rich phytic acid	Microwave	9	400/525	21.65	Wang et al., 2014



B	Hydroquinone and Boron tribromide	Hydrothermal	16	368/500	14.8	Shan et al., 2014
N & B	N-(4-hydroxyphenyl)glycine and boric acid	Hydrothermal	3-200	400/500	11.44	Jahan et al., 2013
N & S	Citric acid and L-cysteine	Hydrothermal	0.5-3.5	345/415	73	Dong et al., 2013

#### 2.1.4 Surface passivation

Surfaces of CQDs possess high sensitivity to contaminants in their environment, such that their properties are easily affected by tiny levels of contaminants. Surface passivation is an effective method to increase the durability and photostability CQDs by the formation of a thin insulating layer, usually by the attachment of passivation agents on an acid-treated CQD surface. The common passivation agents are non-emissive polymers such as PEG, polyethyleneimine (PEI), poly (ethylenimine)-co-poly (ethylene glycol)-co-poly (ethyl-enimide) (PPEI) and 4,7,10-trioxa-1,13-tridecanediamine (TTDDA). It was shown that effective surface passivation is an essential step to produce CQDs with high fluorescence intensities (Lim et al., 2015).

Sun et al., (2006) used diamine-terminated oligomeric polyethylene glycol (average  $n \sim 35$ , PEG<sub>1500N</sub>) as surface passivation agent to synthesize the passivated CQDs, which are strongly photoluminescent both in solution suspension and in solid state, and the emissions cover the visible wavelength range and extend into the near-infrared. Mechanistically, the PL of CQDs was attributed to the surface energy traps, which were caused by plenty of functional groups such as  $-NH_2$  on the surface of CQDs that emitted light upon stabilization because of the surface passivation.

Wang et al., (2010) synthesized CQDs with PEG<sub>1500N</sub> as passivation agent. After separation, QY of almost 60% was obtained. The optical properties of the CQDs is comparable to some commercial products like CdSe/ZnS QDs in solution. Furthermore, Li et al., (2014) prepared a Mg/N co-doping CQDs. The results show that the quantum yield of this co-doped CQDs can reach to 83 %. The PL improvement of the co-doped CQDs is contributed to Mg and preserving the carboxyl group.

## **2.2 CQD-Based Composite Materials**

CQDs demonstrate great potential to replace semi-conductive QDs in applications of energy conversion, sensors, bio-imaging and bio-diagnosis due to their good biocompatibility and excellent optical properties. To stabilize CQDs as well as to improve their optical performances, it is necessary to combine them in an appropriate solid matrix or prepare in solid-state nanocomposites through electrostatic interactions, covalent bonds, non-covalent bonds or hydrogen bonds. A brief review on the CQD-based composite materials will be presented in this section.

### **2.2.1 CQD-incorporated polymeric hydrogels**

Design and synthesis of polymeric nanocarriers with imaging and therapeutic modalities has been of primary significance for the application of cancer nanotheranostics, circumventing the drawbacks associated with conventional cancer diagnosis and treatment. Compared to other nanocarriers, hydrogels possess unique physical properties such as robustness, porosity, tunable cross-linking density, swelling behavior and stability in biological milieu. Therefore, embedding CQDs into polymeric hydrogels is a wonderful technique to prepare fluorescent hydrogels for sensing, bioimaging and cancer nanotheranostics.

Sachdev et al. (2016) designed CQD-incorporated chitosan (CQDs@CTS) hydrogels loaded with an anticancer drug named 5-fluorouracil for drug delivery and bio-imaging modalities. The obtained hydrogels showed excellent functional features such as high surface area, good mechanical strength, swelling behavior together with pH dependent drug release. CQD-incorporated nanogels (CQDs@PEG-CTS) were prepared by complexing CQDs with PEG and chitosan (CTS) via precipitation method (Wang et al., 2015). CQDs@PEG-CTS were used as both carrier for drug doxorubicin and

fluorescent pH probe due to the excellent fluorescence performance and cellular imaging capability provided by CQDs as well as the high loading capacity of drug bestowed by PEG-CTS.

Agarose/CQDs (Agr/CQDs) hydrogels were prepared by microwave-assisted method (Gogoi et al., 2015). Agr/CQDs hydrogels, in which CDs and agarose are linked by electrostatic interaction between amino group and hydroxyl groups, were used as a sensor to detect five transition metals by forming colored chelates with transition metals. Recently, a pH-sensitive CQDs/CTS nanocomposite was fabricated by the solvent casting method for wound dressing application (Omid et al., 2017). The results indicated that the CQDs/CTS hydrogels were biocompatible and nontoxic with effective antibacterial properties. Moreover, the CQDs/CTS hydrogels also demonstrated outstanding pH-sensitive properties, making them an ideal smart material for antibacterial wound healing bandage.

### **2.2.2 CQD- loaded polymeric films**

As functional materials, luminescent films have a wide range of applications in terms of displays, light-emitting devices, safety signs and sensors. Due to the high quantum efficiency, CQDs were increasingly conjugated in polymer composite films for different uses (Zhou et al., 2017).

Chen et al., (2015) reported a white-light-emitting polymer composite film synthesized by conjugating CQDs and lanthanide complexes into a poly (methyl methacrylate) (PMMA) matrix. The synthesized CQDs emitted blue PL while the lanthanide complexes exhibited red and green PL. The obtained high-transparent composite film emitted pure white PL by adjusting the molar ratio of CQDs and lanthanide complexes in the PMMA matrix. Bhunia and her co-workers (2016) fabricated tunable light-

emitting CQDs/PDMS films through one-pot synthesis of *polydimethylsiloxane (PDMS)* matrices with embedded CQDs assembled *in situ*. The fabricated films exhibited different luminescent colors by incorporating CQDs with distinct fluorescence emission profiles produced by different carbon precursors.

Zeng & Yan (2015) prepared a luminescent nanocomposite film by mixing cellulose and CQDs in aqueous solution. The resultant cellulose/CQDs composite film demonstrated extremely high elongation and strong tensile strength with the elastic modulus and tensile strength being 344 and 58.5 MPa, respectively. The good mechanical and transparent properties of the composite film make it a biocompatible material with potential applications in biomedicine, environmentally benign packaging and optical devices. Moreover, Konwar et al., (2015) employed a facile method to prepare CTS/CQDs nanocomposite hydrogel films, in which chitosan and CQD were linked by the electrostatic interaction of positive charge on chitosan and negative charge on CQDs. The composite hydrogel films have fantastic properties on UV–visible blocking, thermal stability and mechanical strength, indicating great potential in the biomedical applications.

Apart from high PL efficiency, the good electrical conductivity of CQDs can also be utilized to fabricate conducting composite films. Pal et al., (2016) firstly prepared a conducting nanocomposite consisting of CQDs and polypyrrole (PPy). The conductivity of the CQDs was explained by the presence of  $sp^2$  C-C bonds which allowed conjugation of the adjacent  $\pi$ -bonds to form the  $\pi$ - and  $\pi^*$ -bands (Eda et al., 2010). And the further incorporation of CQDs into PPy matrices revealed the higher conductivity of the composite film as compared to PPy. The composite film also showed high sensitivity to the presence of picric acid, a widely used organic compound and a

contaminant in groundwater and soil, making it suitable for versatile sensing applications especially in flexible nanoelectronics.

### **2.2.3 CQD-loaded metallic semiconductors**

Metallic semiconductors have been extensively utilized in photocatalysis, which plays an important role in the sustainable energy development and environmental pollution control. However, narrow band gap of metallic semiconductors (e.g. TiO<sub>2</sub> and ZnO) makes them only active in UV light, a minor fraction of the total solar radiation reaching the Earth's surface. Doping nanoclusters on semiconductors has been proved to extend the light absorption of these semiconductors to visible-light and infrared irradiations. On the other hand, although CQDs can act as both electron donors and electron acceptors, which makes them a potential catalyst, there are limited studies on using CQDs directly as photocatalysts.

Alternatively, high-efficient photocatalysts have been developed by incorporating CQDs into metallic semiconductors (Rani et al., 2020). Loading CQDs on semiconductors can effectively improve their photo-catalytic performance under visible light.

The CQDs/semiconductor photocatalysts can be fabricated via either one-pot or multi-step synthetic approach (Chu et al., 2019). With the one-pot approach, all starting materials for the composite are mixed together for further treatment. For example, Wang et al (2015) fabricated the hybrid CQDs/TiO<sub>2</sub> photocatalyst with one-pot synthetic method by hydrothermally treating a mixed solution of sodium citrate and hydrogen fluoride containing Ti foil. CQDs (size ~ 10 nm) were found to uniformly deposit on surfaces of the anatase TiO<sub>2</sub> crystal particles. The obtained CQDs/TiO<sub>2</sub> hybrid significantly enhances the photocatalytic degradation of Rhodamine B under

visible light irradiation. More commonly, the CQDs/semiconductor photocatalyst can be synthesized via multi-step process, by incubating CQDs and separately prepared photocatalyst particles (Ke et al., 2017; Li et al., 2010; Park et al., 2015) or by treating the photocatalyst precursor solution which contains the pre-made CQDs (Li, et al., 2018; Liu et al., 2014; Yu et al., 2012, Zhu et al., 2017; Wang et al., 2018). Compared with one-pot synthesis, multi-step synthetic route provides more flexibility in tuning CQD properties, leading to the enhanced photocatalytic performance.

The up-conversion photoluminescence (UCPL) emission of some CQDs known to be an optical phenomenon wherein materials emit shorter wavelength light than the excitation source, is the main course of extending the sunlight absorption of wide bandgap semiconductors into the visible region and even the near infrared region (Wang et al., 2017). In addition, CQDs are both excellent electron donors and acceptors, which leads to efficient separation of electrons and holes. As such, CQDs can simultaneously serve as electron mediator, photosensitizer, spectral converter, and sole catalyst in photocatalyst design.

### **2.3 Characterization of CQDs and CQD-Based Composite Materials**

Multiple analytical methods can be exploited to characterize CQDs and CQD-based composite materials for the useful information on their size, morphology, structure and optical properties. Among various methods, Fourier transform infrared spectroscopy (FTIR), transmission electron microscopy (TEM), UV/Vis and fluorescence spectroscopies are the most widely used.

#### **2.3.1 FTIR**

Infrared (IR) spectroscopy is one of the most powerful analytical methods available in materials science. It can be applied to both liquid and solid samples and can be used to

analyze both bulk samples and surfaces. When the frequency of infrared light focused through or on a sample identically matches the frequency of stretching or bending vibrations of any pairs of atoms in a molecule, the sample can absorb some of this light. The resulting infrared spectrum can thus provide a great deal of information on the chemical structure of the molecule (Weldon 2012). Many compounds can be identified by the characteristic IR bands of common functional groups.

Fourier transform infrared (FTIR) spectroscopy has been intensively employed to characterize CQDs or CQD-based nanocomposites due to its high speed and sensitivity. As most of the CQDs were prepared by partial oxidation of carbon precursors, the surface of CQDs is rich in hydroxyl, epoxy/ether, carboxyl or carboxylic acid groups. Peng et al. (2012) reported the infrared spectrum of CQDs prepared by chemical oxidation of the micron-sized carbon fibers. Characteristic IR bands of CQDs at  $3307\text{ cm}^{-1}$  and  $1724\text{ cm}^{-1}$  correspond to O–H and C=O stretching vibrations, suggesting the presence of hydroxyl and carboxyl groups. Adsorption peak at  $1579\text{ cm}^{-1}$  is attributed to C=C stretching vibration, whereas band peak at  $1097\text{ cm}^{-1}$  implies the existence of ether (C–O) linkage.

IR spectra for heteroatom-doped CQDs were also studied by many researchers. Absorption peaks at  $3000\text{ cm}^{-1}$ ,  $1580\text{ cm}^{-1}$  and  $1400\text{ cm}^{-1}$  were observed from the FTIR spectrum of N-doped CQDs, which are attributed to the N–H stretching, in-plane N–H bending and amide C–N stretching vibrations respectively (Yang et al., 2017). FTIR spectrum of one-step synthesized S-doped CQDs displayed the absorption bands of O–H at  $3435\text{ cm}^{-1}$ , C–O at  $1715\text{ cm}^{-1}$ , C–C at  $1630\text{ cm}^{-1}$ , S–O/C–O at  $1171\text{ cm}^{-1}$ , and C–S/C–O at  $1043\text{ cm}^{-1}$  (Hu et al., 2014). Characteristic IR bands were also clearly observed from FTIR spectrum of N, S co-doped CQDs (NS-CQDs), including



coalesced O–H and N–H stretching vibrations at  $3378\text{ cm}^{-1}$ , C=O and C–N stretching vibrations at  $1639$  and  $1402\text{ cm}^{-1}$ , C=S and weak C–S stretching vibrations at  $1048$  and  $651\text{ cm}^{-1}$  (Zou et al., 2017).

### **2.3.2 TEM**

TEM is a microscopy technique in which a high energy beam of electrons is shone through a very thin specimen, and the interactions between the electrons and the atoms can be used to observe features such as structure and morphology of the specimen. With a significant role in material sciences, physics, chemistry, and biology, TEM is one of the most widely applied structural analysis tool to date.

High-resolution TEM (HRTEM) is capable of visualizing a sample to the angstrom scale and can thus be used to observe the morphology and size distributions of CQDs (typically with the particle size of 1-10 nm). Shinde and Pillai (2012) prepared CQDs via electrochemical method from multi-walled carbon nanotubes, both interlayers spacing and in-plane lattice spacing of CQDs were observed in the HRTEM image. Microstructures of the CQDs synthesized from biomass were investigated by HRTEM, from which a uniform size distribution (ranging from 1.5 to 4.0 nm) of CQDs and lattice fringes with inter-planar spacing of 0.20 nm were clearly shown (Jing et al., 2019). TEM images of N-doped CQDs exhibited monodisperse nanoparticles (particle size of 2.8-6.3 nm) with near spherical shape and an interlayer spacing of about 0.21 nm (Yang et al., 2017).

### **2.3.3 UV/Vis spectroscopy**

The chemical and electronic structures lay the foundation for the optical properties of CQDs, mainly including optical absorption, PL, and photo-induced electron transfer properties. The optical absorption of CQDs is usually characterized by UV/Vis

spectroscopy. Basically, spectroscopy is related to the interaction of light with a matter. When light is absorbed by a matter, this results in the excitation of the electrons from the ground state towards a higher energy state. The absorption of ultraviolet or visible light by a chemical compound will produce a distinct spectrum. UV/Vis spectroscopy can thus be used to detect the absence or the presence of chromophore in a complex compound.

CQDs usually show strong ultraviolet (UV) absorption, but the positions of UV absorption peaks are quite different for CQDs prepared by different methods. Li and co-workers (Li et al., 2011) prepared water-soluble CQDs by ultrasonic-assisted oxidation of activated carbon. The obtained CQDs demonstrated a UV/Vis absorption at 250~300 nm region, representing the typical absorption of an aromatic  $\pi$  system. Wang et al. (2011) synthesized CQDs by the solvothermal method from citric acid at 240 °C. Highly luminescent (quantum yield=47 %) amorphous CQDs that exhibited a strong absorption peak at 360 nm in the UV/Vis absorption spectrum were obtained. Hu et al., (2014) synthesized NS-CQDs using a microwave-assisted hydrothermal method from rice powder and *N*-acetyl-*L*-cysteine. Unlike the undoped CQDs, which showed a sharp UV adsorption peak at 275 nm corresponding to the  $n \rightarrow \pi^*$  transition of C=O bond, the NS-CQDs demonstrated a prominent absorption peak at 335 nm probably due to the formation of excited defect surfaces induced by the N and S heteroatoms. Recently, Lan and co-workers (Lan et al., 2017) prepared S, Se-codoped CQDs via hydrothermal method and the resultant CQDs had broad absorption from 350 to 750 nm with a maximum peak at ~526 nm, rendering the near-infrared (NIR) emissions of the prepared CQDs.

### 2.3.4 Fluorescence spectroscopy

The photoluminescence (PL) of CQDs can be characterized by fluorescence spectroscopy (FS). FS uses a beam of light that excites the electrons in molecules of certain compounds and causes them to emit light. With most spectrofluorometers, it is possible to record both excitation and emission spectra. An emission spectrum is the wavelength distribution of an emission measured at a single constant excitation wavelength. Conversely, an excitation spectrum is the dependence of emission intensity, measured at a single emission wavelength, upon scanning the excitation wavelength (Lakowicz, 2006).

One unique PL property of CQDs is their clear excitation-dependent emission wavelength and intensity. For example, passivated CQDs fabricated by hydrothermal method exhibited strong blue luminescence under 365 nm excitation. The emission spectra of the CQDs were broad, ranging from 430 to 580 nm. The excitation-dependent PL emission of the prepared CQDs can be attributed to the presence of surface energy traps stabilized by surface passivation (Liu et al., 2009). Highly luminescent CQDs (QY = 47%) prepared by solvothermal method demonstrated emission peaks at 460, 540 and 620 nm when excited at 380, 460 and 540 nm separately, indicating the dependence of the maximum emission on the excitation wavelength (Sun et al., 2015).

Recently, excitation-independent fluorescent CQDs were fabricated by self-controlled methods. In the fluorescence spectra, CQDs showed an excitation-independent emission peak at 407 nm with bandwidth of ~61 nm (Zuo et al., 2014). The authors ascribed the phenomenon to the occurrence of fluorescence resonance energy transfer, a non-radiative energy transfer between an excited donor and an acceptor through dipole-dipole interactions. Excitation-independent emission was also observed from N-

doped CQDs derived from different amino acids (Wei et al., 2014). The Trp-CQDs and Asp-CQDs emitted blue light around 450 nm and yellow light around 560 nm, respectively, indicating that their emissions were excitation independent. The authors speculated that the excitation-independence of Trp-CQDs and Asp-CQDs were due to the narrow size distributions and their uniform chemical surfaces.

### **2.3.5 XPS**

X-ray photoelectron spectroscopy (XPS) is an important surface analyzing technique of the material. The empirical formula, elemental composition, electronic state, and chemical state of the elements can be measured by XPS within a material. XPS spectra are acquired by irradiating a solid surface with a beam of X-rays while at the same time gauging the kinetic energy (K.E.) of electrons discharged from the highest 1-10 nm of the substance being analyzed. A photoelectron spectrum is recorded by counting ejected electrons over a range of electron as kinetic energies. Peaks show up in the spectrum from atoms that emit a specific characteristic energy's electrons. The intensities and energies of the photoelectron peaks allow quantification and identification of all surface elements except for hydrogen and helium (Van der Heide, P., & ProQuest. (2012).

Li et al., (2013) synthesized CQDs using the thermal pyrolysis method from soya bean grounds. They observed that only 1.33% nitrogen atomic content with binding energy at 400 eV. Furthermore, the high-resolution C1s spectra exhibited strong signals at 286.0 eV that attributed to carbon atoms (C-O, C-N and C=C) consisting of FTIR measurement outcomes. As expected for biomedical application, there were varying organic functional bands on C-dots surface, endowing them with not only hydrophilicity but also photostability

## **2.4 Applications of CQD-Based Functional Materials**

### **2.4.1 Bioimaging**

Bioimaging is one of the major areas where CQDs and CQD-incorporated polymeric hydrogels are widely used. Bioimaging is a noninvasive process of visualizing biological activity in a specific period. It helps to gain information on the 3-D structure of the observed specimen from the outside without physical interference. Bioimaging spans the observation of subcellular structures and entire cells over tissues up to entire multicellular organisms. Because of their tunable multicolor emission and low toxicity, CQDs and CQD-based materials have played an essential role as a platform for cancer nanotheranostics, an integrated diagnostic and therapeutic approach for cancer treatment.

For fluorescence (FA) imaging probes, red or near-infrared (NIR) emissive (>600 nm) CQDs are favorable due to their deep tissue penetration, minimal tissue absorption, minimal photodamage, and low autofluorescence interference to biological samples (Jia et al., 2020). Ko et al., (2013) prepared NIR fluorescence emitting CQDs from tire soot through nitric acid oxidation and used them as imaging agents for living cells. Ruan et al., (2014) investigated the potential of CQDs for imaging of glioma tumors. The fabricated CQDs exhibited highest emission peak at 500 nm and have shown high ability to selectively localize glioma cells in the brain rather than normal tissues, suggesting the fabricated CQDs can be applied as potential candidates for the brain glioma tumor treatments without any toxic effects to normal cells. Most recently, Hao and coworkers reported a new type of CQDs with NIR-II (1100–1600 nm) emission by using environment-friendly watermelon as a precursor via a one-step hydrothermal reaction (Li et al., 2019). The obtained CQDs displayed an emission peak of 900–1200

nm under 808 nm laser irradiation. Results from *in vivo* bioimaging test indicated that strong NIR-II FL signals were observed in the kidney within 1 min post-intravenous CQD injection.

CQDs have also been widely constructed as reagents for two-photon fluorescence imaging (TPFI), which has received great attention in basic biological research and clinical diagnostics because of its large penetration depth, autofluorescence background, and reduced photodamage in tissues. In 2007, Sun and co-workers first used surface-passivated CQDs with a high two-photon absorption for multiphoton imaging (Gao et al., 2007). Subsequently, N-doped CQDs synthesized by using dimethylformamide as nitrogen source and solvent were used as effective TPFI probes for cellular and deep-tissue imaging (Liu et al., 2013). A large penetration depth of 1800 mm can be achieved by N-CQDs in a tissue phantom, significantly extending the fundamental TPFI depth limit. In 2018, three-photon-induced red emission was observed from CQDs prepared by the surface engineering of molecules or polymers rich in sulfoxide/carbonyl groups (Li et al., 2018).

CQDs can be combined with other materials for bimodal or multimodal imaging as well. For example, Jia et al. (2016) designed a multifunctional nanoplatform of gold nanorod@silica-CQDs (GNR@SiO<sub>2</sub>-CQDs), in which GNRs act as photoacoustic (PA) imaging and photothermal therapy (PTT) agents with 808 nm laser, and CQDs serve as fluorescence imaging and photodynamic therapy (PDT) agents with 635 nm laser. Highly- sensitive and high-resolution bimodal FL/PA images of tumor demonstrate that GNR@SiO<sub>2</sub>-CDs can gradually accumulate in tumors after intravenous administration. However, problems on requiring two light sources for synergistic PTT/PDT and high laser power for PTT remain unsolved. Later on, the same research group prepared a

type of NIR CQDs from polythiophene benzoic acid. The obtained CQDs not only exhibit red-light emission (640-680 nm), but also show dual PDT and PTT effects. This study first reported the utilization of CQDs for *in vivo* imaging-guided synergistic PDT/PTT by using a single laser (Ge et al., 2016).

#### **2.4.2 Sensing**

Functional CQDs have been employed as chemosensors for the detection of various analytes including chemical pollutants and biologically active small molecules. The interaction of CQDs with analytes results in subsequent changes of fluorescence turn-on (enhancement) or turn-off (quenching) observed in the CQDs (Molaei, 2020). Detection mechanisms such as photoinduced electron transfer (PET), fluorescence resonance electron transfer (FRET), aggregation-induced red-shift emission (AIRSE), and inner filter effect (IFE) have been employed to explain the basic principles of CQD sensors.

CQDs have emerged to be precise sensors for metal ions with the limit of detection (LOD) in the micromolar, nanomolar, or even picomolar scales (Dhenadhayalan et al., 2020). Detection of metal ions is the most important worldwide task to monitor and control the environmental pollution. The most commonly used methods for metal detection such as AAS, ICP-OES and ICP-MS, are all need for large-scale, costly instruments, and complicated synthesis process of sensing materials. However, CQDs as novel fluorescence sensors possess the advantages of intrinsic simplicity, high sensitivity and selectively, low cost and simple instruments requirement (Lu et al., 2018).

Surface functional groups (e.g. carboxyl, hydroxyl and amino) of CQDs effectively interact with metal ions through surface bonding, resulting in the tuning of CQD

properties. Table 2.3 summarizes the recent research studies on the applications of chemical-derived CQDs in heavy metal sensing.

Table 2.3 Metal ion sensing by chemical-derived CQDs

<b>CQD materials</b>	<b>Analytes</b>	<b>Mechanisms</b>	<b>LOD</b>	<b>Ref.</b>
CQDs	Au <sup>3+</sup>	Off - IFE	3.35 $\mu$ M	Gao et al., 2019
CQDs	Pb <sup>2+</sup>	ET	0.59 nM	Kumar et al., 2017
CQDs	Se (IV)	IFE; ET	0.78 $\mu$ M	Devi et al., 2017
N-CQDs	Hg <sup>2+</sup>	PET	0.201 $\mu$ M	He et al., 2016
N-CQDs	Hg <sup>2+</sup>	ET	2.8 nM	Wang et al., 2019
N-CQDs	Cu <sup>2+</sup>	FRET	23 nM	Zhang et al., 2019
CQDs@quercetin	Zn <sup>2+</sup>	FRET	2 $\mu$ M	Yang et al., 2015
CQDs@Eu-DPA	Cu <sup>2+</sup>	OFF	26.3 nM	Hao et al., 2017
MOFs				
CQDs@AuNCs	Cd <sup>2+</sup>	IFE	32.5 nM	Niu et al., 2016
N-CQDs@cytopore	Cd <sup>2+</sup>	Solid phase extraction	201 nM	Li et al., 2018
NS-CQDs	Hg <sup>2+</sup>	IFE	0.18 $\mu$ M	Wang et al., 2015
NS-CQDs	Fe <sup>3+</sup>	ET	0.27 $\mu$ M	Yang et al., 2019

Notes: LOD: limit of detection; IFE: inner filter effect; ET: electron transfer  
FRET: fluorescence resonance energy transfer

Apart from metal ion sensing, growing applications of CQDs to the detection of biomolecules have been reported (Hu et al., 2014; Wei et al., 2014). Lu et al., (2018) investigated the detection of L-cysteine using N-doped CQDs along with Fe<sup>3+</sup>. Experimental results showed that the strong fluorescence of N-CQDs was quenched upon the addition of Fe<sup>3+</sup> ions and then the fluorescence was recovered followed by the addition of L-cysteine. Due to the strong interaction between L-cysteine and Fe<sup>3+</sup>, this N-CQDs/Fe<sup>3+</sup> system demonstrated excellent selectivity and sensitivity with LOD of 0.27  $\mu$ M. Zhou et al., (2018) reported the detection of hemoglobin using a fluorescent nano-biosensor which is based on the molecularly imprinted polymers and CQDs by



means of the fluorescence quenching. The fabricated biosensor exhibited an extremely low LOD (0.77 nM) of hemoglobin with excellent sensitivity and high selectivity.

Moreover, CQDs along with metal nanoparticles were functioned as a sensing platform in the detection of pesticides and other organic pollutants. Detailed review on this application has been conducted by Dhenadhayalan and co-workers (Dhenadhayalan et al., 2020).

### **2.4.3 Photocatalysis**

The CQD-incorporated semiconductor photocatalysts have been applied to various photocatalytic reactions, such as photo-degradation of organic pollutants, water splitting and CO<sub>2</sub> conversion.

CQD-based photocatalysts for degradation of dyes and organic pollutants have been intensively studied. Li et al., (2010) firstly reported the utilization of CQDs/TiO<sub>2</sub> and CQDs/SiO<sub>2</sub> in degradation of methylene blue (MB) with 300W halogen lamp. The minimum degradation of MB in the absence of CQDs confirmed their participation in dye degradation and their interaction with TiO<sub>2</sub> or SiO<sub>2</sub>. Tian et al., (2015) fabricated a CQD/hydrogenated TiO<sub>2</sub> (CQD/H-TiO<sub>2</sub>) nanobelt heterostructure to remove organic contaminants under UV, visible, and near-infrared irradiation. More than 86% removal rate of organic pollutant was achieved within 25 min of reaction by using CD/H-TiO<sub>2</sub> heterostructure as catalyst, which is found to be superior to those by pure TiO<sub>2</sub> nanobelt (63%) or H-TiO<sub>2</sub> nanobelt (82%).

Development of CQD-incorporated semiconductors for solar water splitting has gained immense attention in recent years (Mehta et al., 2019). Hydrogen obtained from photocatalytic water splitting using sunlight can be highly clean and is a sustainable

energy source compared to conventional fossil fuels. Yu et al., (2014) prepared a CQDs/TiO<sub>2</sub> composite with efficient photocatalytic H<sub>2</sub> evolution activity via a facile one-step hydrothermal strategy. Under UV-Vis light irradiation, the photocatalytic H<sub>2</sub> evolution rate of CQDs/TiO<sub>2</sub> is 9.1 μmol h<sup>-1</sup>, about 4 times higher than that of pure TiO<sub>2</sub>. Pan et al. (2018) synthesized CQD-modified g-C<sub>3</sub>N<sub>4</sub>/TiO<sub>2</sub> nano-heterojunctions via a facile hydrothermal method. The nano-heterojunctions exhibited nearly two orders of magnitude enhancement in H<sub>2</sub> production compared with those of unmodified catalysts (C<sub>3</sub>N<sub>4</sub>/TiO<sub>2</sub>, CQDs/TiO<sub>2</sub>). Superior properties of CQDs, including their large storage capacity of electrons and their unique UCPL contribute to the enhancement in photocatalytic hydrogen production.

## Chapter 3 One-Pot Synthesis of N-Doped CQDs

### 3.1 Introduction

Nowadays, the hydrothermal method has been widely employed to fabricate carbon quantum dots (CQDs), a class of environmentally-friendly photoluminescence (PL) nanomaterials with potential applications in the fields of biomedical imaging, optoelectronics, chemical sensing and photocatalysis. Through pyrolysis or carbonization of carbon precursors under high temperature conditions, hydrothermal method is capable of producing CQDs from a variety of carbon precursors such as small organic molecules (e.g. glucose, amino acids, citric acid) and natural biomass materials (e.g. watermelon peel, pomelo peels, carbohydrates). However, CQDs obtained from one-pot hydrothermal method are typically with heterogeneous structures and indefinite composition, resulting in low quantum yield (QY) and emission peak shift with increasing excitation wavelength (Mishra et al., 2019).

Bottom-up hydrothermal synthesis of CQDs from small molecules or polymers is an efficient pathway to produce CQDs in large scale. Citric acid (CA) is the most common reagent to synthesize CQDs through bottom-up method (Zhu et al., 2016). Compared with CQDs synthesized from biomass materials, fluorescent CQDs prepared from CA possess a number of advantages such as biocompatibility, stable photoluminescent property and high quantum yield (Kasprzyk et al., 2018). It has been experimentally proved that the PL of CA-based CQDs can be enhanced through doping and/or surface passivation using amine-based agents, such as ethylenediamine (EDA), cysteine, polyethyleneimine and glutathione (Song et al., 2015). Heteroatom doping and/or surface passivation can not only enhance the fluorescent properties of CQDs (e.g.,

increased QY, tunable emission wavelength, etc.) but also, significantly increase the durability and photostability of CQDs (Kim et al., 2018; Lim et al., 2015).

Although considerable research has been devoted to the synthesis of CQDs from CA using hydrothermal method, few of them have been focused on the optimization of the hydrothermal reactions. Generally, optimization of hydrothermal reactions can be beneficial on several different fronts, and the most important ones are the highest attainable QY and the lowest energy consumption. Design of experiments (DOE) is a systematic method to determine the relationship between factors affecting a process and the output of that process (Niedz et al., 2016). It allows for multiple input factors to be maneuvered, determining their effects on a desired output (response). By manipulating multiple inputs at the same time, DOE can identify important interactions that are omitted in the one-factor-at-a-time method. Among different DOE methodologies, Box-Behnken design (BBD) is a class of rotatable or nearly rotatable second-order designs based on three-level incomplete factorial designs (Garg et al., 2016). The treatment combinations in this design are the midpoints of edges of the process space and at the center. Compare to the Central Composite design (CCD), the key feature of the BBD is that the number of experimental runs is lower as it does not contain the extreme factor combinations. Moreover, CCD usually have axial points outside the 'cube'. These points may not be in the region of interest or may be impossible to conduct because they are beyond safe operation limits. Thus, it can be sure that all design points of BBD fall within the safe operating zone (Kabuk et al., 2014).

Understanding the origin and mechanism of the fluorescence behavior of CQDs has been a hot topic in recent years. It is widely accepted that CQDs are composed of carbon-core and surface domains (Dhenadhayalan et al., 2016; Xia et al., 2019). The

carbon-core domain is characterized by a  $sp^2$  carbon structure similar to the graphene, whereas the surface domain contains abundant functional groups. Due to the heterogeneous structural nature of the CQDs, it is difficult to explain the specific chemical structure of CQDs and the components contributing to the fluorescence. As such, different fluorescence mechanisms of CQDs in terms of the recombination of electron-hole pairs, quantum effect, surface functional groups, molecular state, and fluorophores with different degrees of  $\pi$ -conjugation have been proposed (Baker and baker, 2010; Bourlinos et al., 2011; Hsu and Chang, 2012; Mao et al., 2020; Zhu et al., 2013). So far, both the recombination of electron-hole pairs (Sahu et al., 2012) and the molecular state (Song, et al., 2015; Zhu et al., 2013) have been broadly accepted as the mechanisms of fluorescence for CQDs. Nonetheless, effective characterization and structural analyses are still needed to elucidate the fluorescence properties of CQDs prepared under different hydrothermal conditions.

In this work, we first optimized the synthetic conditions of N-doped CQDs (N-CQDs) using the BBD, and then characterized the chemical structures and surface states of the as-prepared N-CQDs using TEM, XPS, and FRIR. Finally, the unique optical properties of the N-CQDs were investigated by UV-Vis and fluorescence spectroscopy.

## **3.2 Materials and Methods**

### **3.2.1 Materials**

ACS grade citric acid (CA) anhydrous, 99% ethylenediamine (EDA) and 99% quinine sulfate dehydrate were purchased from Fisher (Canada). These chemicals were used as received without further purification. Deionized (DI) water used for all experiments was generated from Milli-Q water purification system (Millipore Corporation) in the lab.

### **3.2.2 The Preparation of N-CQDs**

For the synthesis of N-CQDs, certain amounts of CA and EDA (based on the required molar ratio of EDA to CA) were added in 40.0 mL of DI water in a 100.0 mL polypropylene-lined stainless-steel autoclave. Hydrothermal reactions were carried out in a programmable oven from Thermo Fisher for 4.0 h. After the autoclave was cooled to the room temperature, the obtained solution was filtered through 0.22  $\mu\text{m}$  membrane filters to remove the large particles, followed by centrifuging at 4000 rpm for 0.5 h. The supernatant was then kept in a dialysis bag in ultrapure water for 4.0 h and finally the solid N-CQDs were collected after freeze-drying.

### **3.2.3 Design of experiments (DOE) for the preparation of N-CQDs**

An experimental design for three factors at three levels was employed to prepare N-CQDs, with the detailed reactions conditions as: the concentration of CA with three levels of 0.4, 0.5, 0.6 mol/L; the temperature with three levels of 180, 200 and 220  $^{\circ}\text{C}$ , and the molar ratio of EDA to CA with three levels of 1:2, 1:1 and 2:1, respectively.

The response is QY. Reaction time and volume are fixed at 4.0 h and 40.0 ml.

The Box-Behnken design for three factors requires 12 experiments plus central point replications. The detailed reaction conditions for different experimental runs are listed in Table 3.1.

Table 3.1 Box-Behnken design

Run	Conc. of CA (mol/L)	Molar Ratio of EDA:CA	Temperature (°C)
1	0.4	1:1	180
2	0.5	1:2	180
3	0.5	2:1	180
4	0.6	1:1	180
5 <sup>a</sup>	0.5	1:1	200
6	0.4	1:2	200
7	0.4	2:1	200
8 <sup>a</sup>	0.5	1:1	200
9	0.6	1:2	200
10 <sup>a</sup>	0.5	1:1	200
11	0.6	2:1	200
12 <sup>a</sup>	0.5	1:1	200
13 <sup>a</sup>	0.5	1:1	200
14	0.4	1:1	220
15	0.5	1:2	220
16	0.5	2:1	220
17	0.6	1:1	220

<sup>a</sup> Runs 5, 8, 10, 12 and 13 are the central point replications of the Box-Behnken design

### 3.2.4 Analytical methods

X-ray photoelectron spectroscopy (XPS) measurements of the as-prepared N-CQDs were performed using a XPS - PHI 5000 VPIII (ULPAC-PHI Inc., Japan). Transmission electron microscopy (TEM) images were recorded with a Tecnai Spirit microscope. The Fourier transform infrared (FTIR) spectra of N-CQDs were measured by a Bruker Tensor II FTIR spectrometer (Bruker, Germany) over a range from 400 to 4000 cm<sup>-1</sup>. A Varian Cary 100 Bio UV-Vis spectrophotometer was used to obtain UV-Vis absorption spectra of N-CQDs dispersed in DI water. Fluorescence spectra of N-CQDs were measured in 1 cm standard quartz cuvette using a PTI-QuantaMaster

spectrofluorometer (Photon Technology International Inc., USA). The pH values were measured using an Accumet pH meter, AB 15<sup>+</sup> (Fisher Scientific, Canada).

### 3.2.5 Determination of quantum yield (QY)

The QY of the C-dots in aqueous solution was measured using quinine sulfate as the reference (54%) and calculated using following Eq:

$$QY_C = QY_R \times \frac{S_C}{S_R} \times \frac{A_R}{A_C} \times \frac{\eta_C^2}{\eta_R^2} \quad (3-1)$$

where,  $QY$  represents the quantum yield value,  $S$  is the fluorescent intensity,  $A$  refers to the absorbance measured at excited wavelength, and  $\eta$  represents the refractive index of the solvent used. The subscripts “C” and “R” refer to N-CQDs and reference sample of known quantum yield, respectively.

If we can ensure that the absorbance of the reference sample and N-CQDs are consistent, and the sample concentrations are extremely low (absorbance value less than 0.05), then Eq. (3-1) can be simplified to:

$$QY_C = QY_R \times \frac{S_C}{S_R} \quad (3-2)$$

## 3.3 Results and Discussion









### 3.3.1 DOE optimization of synthetic conditions








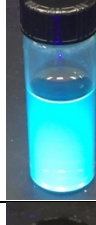






Quantum yields of N-CQDs, at 350 nm excitation ( $\lambda_{ex} = 350$  nm), obtained from 17 experimental runs vary from 19.3% to 52.1%, which is acceptably good compared with those reported from open literature (Wu et al., 2013; Huang et al., 2018; Ding et al., 2014; Zhou et al., 2019). The ANOVA analysis of the experimental results was carried out by using the Design-Expert 11. Results of a first-order model are summarized in Table 3.3, from which the most influential factors ( $p < 0.05$ ) on QY of N-CQDs are

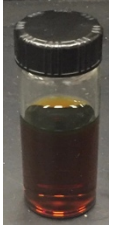





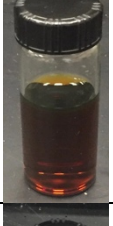







found to be the molar ratio of EDA to CA and reaction temperature. Moreover, the interaction of these two factors also shows influence on QY of N-CQDs. The results from ANOVA analysis describe that initial concentration of citric acid has no significant effect ( $p=0.265$ ) on the attained QY values. All these results clearly indicate that the optimum QY is attainable by tuning reaction temperature and the molar ratio of EDA to CA.

Table 3.2 Reaction conditions for hydrothermal preparation of N-CQDs

Run	Reaction conditions			QY %	Visible light	UV-light
	Conc. of CA mol/L	Molar Ratio of EDA:CA	Temperature °C			
1	0.4	1:1	180.0	51.9		
2	0.5	1:2	180.0	26.9		
3	0.5	2:1	180.0	52.1		
4	0.6	1:1	180.0	47.0		

5 <sup>a</sup>	0.5	1:1	200	41.7		
6	0.4	1:2	200.0	24.5		
7	0.4	2:1	200.0	40.4		
8 <sup>a</sup>	0.5	1:1	200.0	43.0		
9	0.6	1:2	200.0	19.3		
10 <sup>a</sup>	0.5	1:1	200.0	43.0		
11	0.6	2:1	200.0	38.2		

12 <sup>a</sup>	0.5	1:1	200.0	43.0		
13 <sup>a</sup>	0.5	1:1	200.0	41.0		
14	0.4	1:1	220.0	26.6		
15	0.5	1:2	220.0	23.0		
16	0.5	2:1	220.0	47.3		
17	0.6	1:1	220.0	30.5		

<sup>a</sup> These runs represent the central points replications.

Table 3.3 The ANOVA results for the model

Source	Sum of Squares	df	Mean Square	F-value	p-value	
<b>Model</b>	1728.14	11	157.10	28.69	0.0008	significant
Conc. of CA	8.61	1	8.61	1.57	0.2653	
Temperature	318.78	1	318.78	58.21	0.0006	
EDA:CA	1095.48	2	547.74	100.03	< 0.0001	
AB	19.36	1	19.36	3.54	0.1188	
AC	7.36	2	3.68	0.6724	0.5513	
BC	137.15	2	68.58	12.52	0.0113	
A <sup>2</sup>	121.64	1	121.64	22.21	0.0053	
B <sup>2</sup>	7.96	1	7.96	1.45	0.2819	
<b>Residual</b>	27.38	5	5.48			
Lack of Fit	27.38	1	27.38			
Pure Error	0.0000	4	0.0000			

### 3.3.1.1 Effect of temperature

Hydrothermal temperature is an important operating parameter for the synthesis of N-CQDs. As the reaction progresses from low temperature to high temperature, the polymer-like CQDs are changed into carbogenic CQDs (Song et al., 2015). This is understandable, high reaction temperature leads to the carbonization of the organic molecules, which has been confirmed from the color of N-CQDs products as shown in Table 3.2. The color of N-CQDs solutions produced at  $T = 220$  °C are much darker than those produced at  $T = 180$  °C. In most of the cases, N-CQDs with lower QY were obtained when reaction temperature is higher than 200 °C. No significant variations were found from the UV-Vis absorbance peaks and fluorescence emission wavelengths of the N-CQDs synthesized under different hydrothermal temperatures. Therefore, to

produce N-CQDs with high QY, reaction temperature should not exceed 200°C. Results from Table 3.2 indicate that  $T = 180^{\circ}\text{C}$  is the optimum.

### **3.3.1.2 Effect of the molar ratio of EDA to CA**

The molar ratio of EDA to CA has remarkable influence on the QY values of N-CQDs, which can be observed from the results illustrated in Fig. 3.1. In general, the QY of N-CQDs greatly increased with the N content. QY of N-CQDs increased from less than 20.0% to more than 50.0% when the EDA to CA ratio increased from 0.5 to 2.0. However, the degree of influence of EDA to CA ratio on QY varies when combining with different reaction temperatures and/or initial concentrations of CA. With the lower (EDA: CA=0.5) and higher (EDA:CA=2.0) limits, the magnitudes of variation in QY with the reaction temperature are 7.6% (from 19.3% to 26.9%) and 13.9% (from 38.2% to 52.1%), respectively. However, when the intermediate level of EDA to CA (1.0) ratio is used, QY decreases remarkably with the increasing reaction temperature. QY value varies from of 51.9 % at  $T= 180^{\circ}\text{C}$  to 26.6% at  $T= 220^{\circ}\text{C}$ , decreasing more than 25.0%. Based on the reported study carried out by Bai and co-workers (Yang et al., 2017), nitrogen was doped into the carbon framework during the hydrothermal treatment to form the N-CQDs core with graphene-like carbon ring structures. With the prolongation of the reaction, the carbon core was covered by the passivated shell mainly consisting the amino group and the oxygen-containing groups. Typically, carbon core and surface state both significantly contribute to the fluorescence property of the resultant N-CQDs. As such, hydrothermal reaction temperature, reaction time, as well as the EDA to CA ratio must be properly selected so that an optimal balance among the degrees of N-doping, carbonization, and surface passivation can be achieved.

Based on the BBD experimental results, reaction temperature of 180° and EDA to CA ratio of 1.0 are the optimal reaction conditions for the preparation of N-CQDs. Therefore, an extra experiment was done at the optimal reaction conditions and the QY of it is 51.7%.

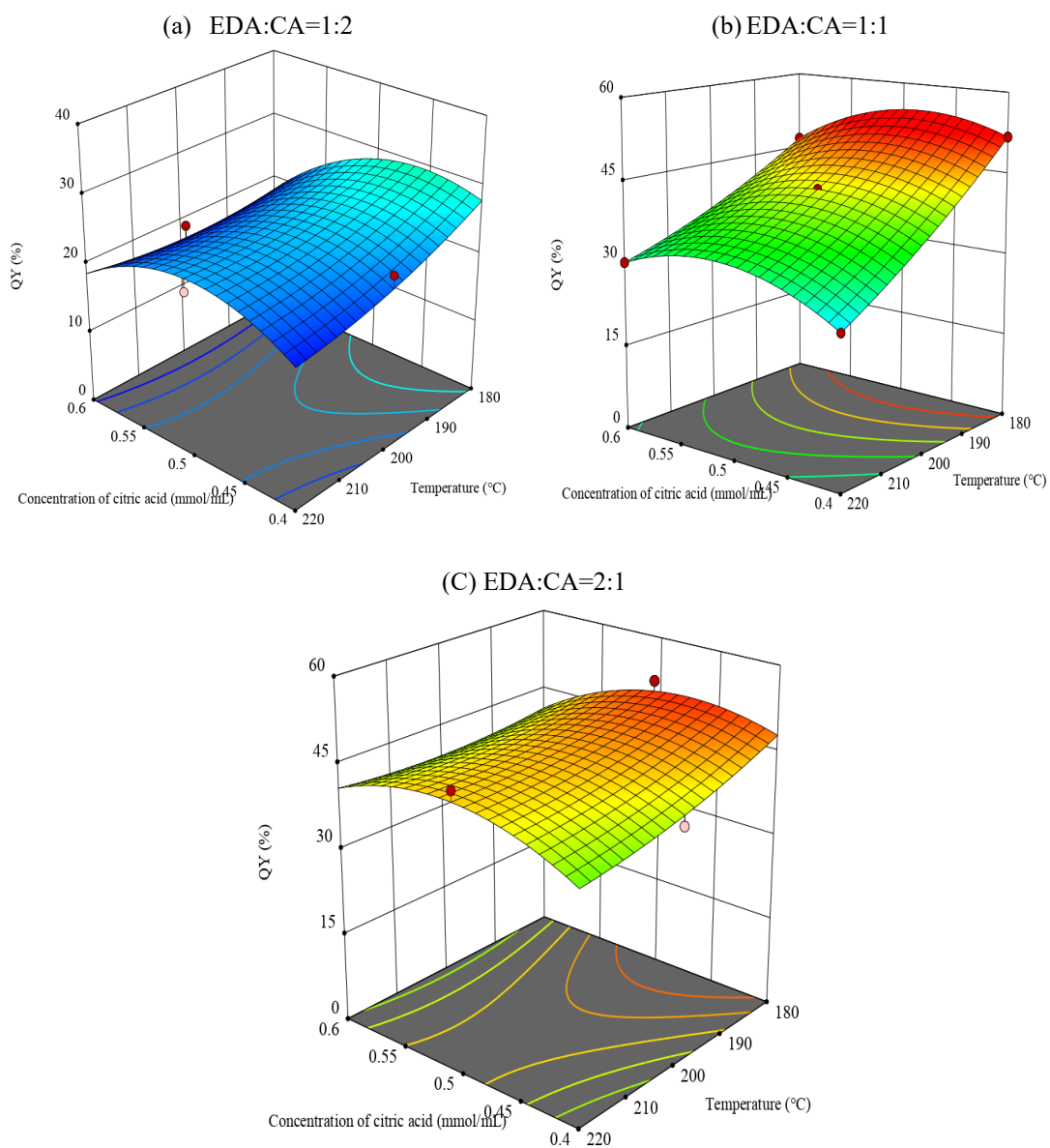


Figure 3.1 The 3D surface under different ratio of EDA:CA

### 3.3.2 Characterization of the as prepared N-CQDs

The morphology and particle size of the N-CQDs characterized by TEM are illustrated in Fig. 3.2, from which well dispersed spherical particles of N-CQDs are observed without significant agglomeration. The average size of the N-CQDs is roughly 20 nm.

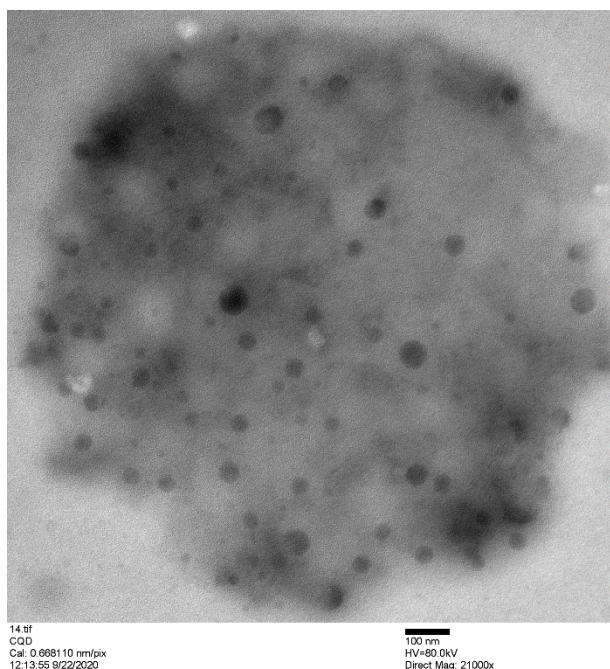


Figure 3.2 TEM image of N-CQDs

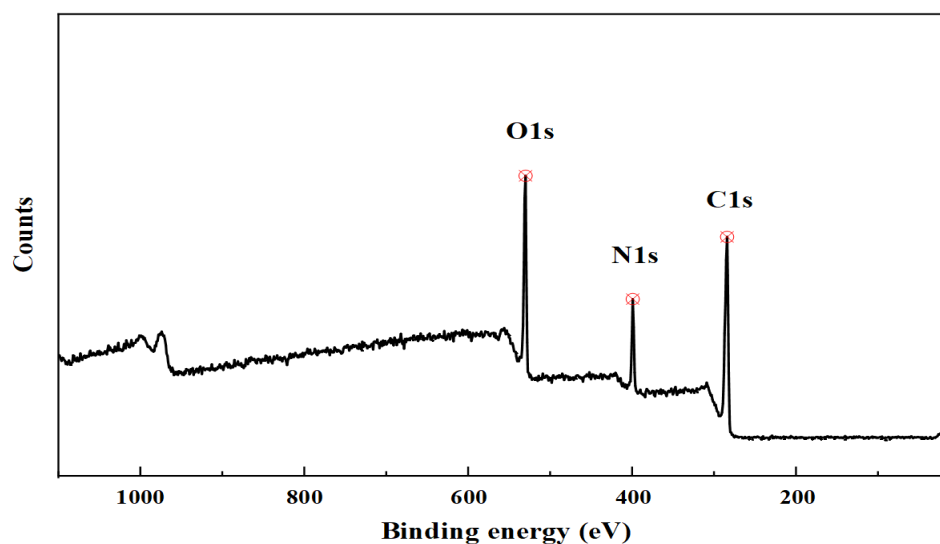


Figure 3.3 XPS survey spectrum of N-CQDs

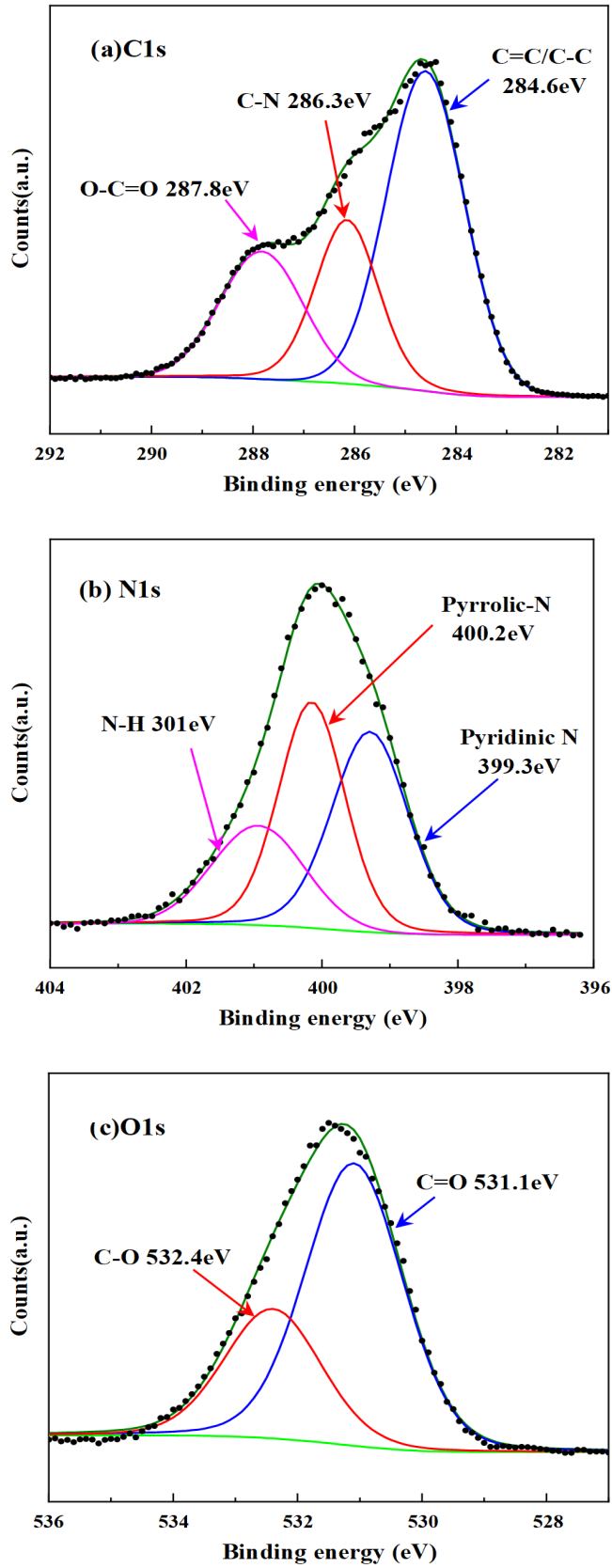


Figure 3.4 High resolution C 1s (a); N 1s (b); and O 1s (c) XPS spectra of N-CQDs



The surface composition and elemental analysis of the N-CQDs were characterized by XPS. The peaks at 284.7, 399.8 and 531.4 eV in a XPS survey spectrum (Fig. 3.3) can be attributed to C 1s, N 1s, and O 1s, respectively.

In the high-resolution spectrum of C1s as shown in Fig. 3.4a, three deconvoluted BE peaks at 284.6, 286.2 and 287.8 eV which are attributed to the  $sp^2$  C (C=C) in graphite, the  $sp^3$  C (C–O and C–N), and the oxidized C (C=O), respectively (Gao et al., 2016; Qu et al., 2014). Three deconvoluted BE peaks at 399.3, 400.2, and 401.0 eV corresponding to the pyridinic N (C–N–C), and the pyrrolic N (C–N, and N–H) were observed for N 1s from Fig. 3.4b. XPS spectrum of N 1s for N-CQDs from this study are consistent with those reported from open literature (Ding and Xiong, 2015; Gao et al., 2016; Wu et al., 2014). The two peaks of the O1s spectrum (Fig. 3.4c) at 531.1 and 532.4 eV are assigned to the C=O, and C–OH/C–O–C groups respectively (Ding and Xiong, 2015; Qu et al., 2014).

Chemical and structural information of N-CQDs was also characterized by FTIR. The IR spectra of citric acid and N-CQDs are compared in Fig. 3.5. Significant band shifts take place within the regions of 3200-3700  $cm^{-1}$  and 1200-1700  $cm^{-1}$ . For citric acid, the characteristics IR bands include: alcohol and acid O–H stretching at 3491 and 3285  $cm^{-1}$ ; carboxylic C=O stretching at 1745 and 1694  $cm^{-1}$ ; and acyl and alkoxy C–O stretching at 1170 and 1137  $cm^{-1}$  (Pimpang et al., 2018). Instead, a broad peak at 3245  $cm^{-1}$  is observed from the IR spectrum of N-CQDs, which is due to the coalescing effect of the stretching vibrations of O–H, N–H and C=C–H. Characteristic peaks at 1696, 1647 and 1532  $cm^{-1}$  are attributed to the stretching vibrations of carboxylic C=O, C=N and C=C in aromatic rings, respectively (Holá et al., 2017). In addition, IR band of N-CQDs at 1211  $cm^{-1}$  can be ascribed to the stretching vibration of C–N. These results

indicate that N-CQDs consist of graphite structures in the cores and amorphous carbon on the surface, similar with those previously reported CQDs (Holá et al., 2017; Song et al., 2015).

It is very difficult to investigate the formation mechanism of the N-CQDs because various reactions are involved during the hydrothermal reaction process. In a similar system employing CA and amines, Sun and co-workers (Qu et al., 2014) reported that the formation of the N-CQDs involved two steps. Firstly, with the help of amines, the CA molecules self-assembled into a sheet structure and dehydrolyzed to form a graphene framework. Meanwhile, amidation took place between the CA and the amine molecules. Secondly, amides reacted with the neighboring carboxylic groups to form a pyrrolic N species through intramolecular dehydrolysis (Dong et al., 2012). The XPS and FTIR results of the N-CQDs from the current study confirm the occurrence of the above-mentioned reactions.

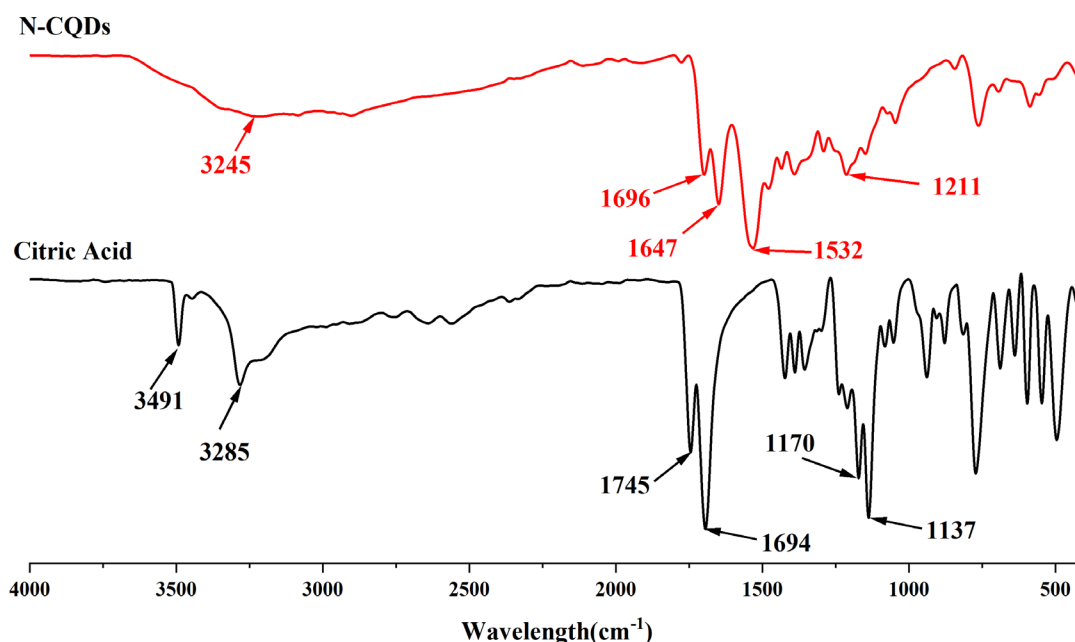


Figure 3.5 FTIR spectra of CA and N-CQDs

### 3.3.3 Optical properties of N-CQDs

UV-Vis absorbance spectrum of N-CQDs is illustrated in Fig 3.6, from which two obvious absorption peaks at 345 nm can be observed. The absorption peak at 345 nm is due to the  $n-\pi^*$  transitions of C=O or C-OH bonds present in the N-CQDs. The fluorescence spectrum of N-CQDs can also be seen from Fig. 3.6, which indicates that the optimal emission wavelength of N-CQDs is 460 nm. It should be noted that neither citric acid nor ethylenediamine solution emits luminescence in the visible region at an excitation wavelength ( $\lambda_{ex}$ ) of 350 nm, revealing that the bright blue fluorescence originates from N-CQDs.

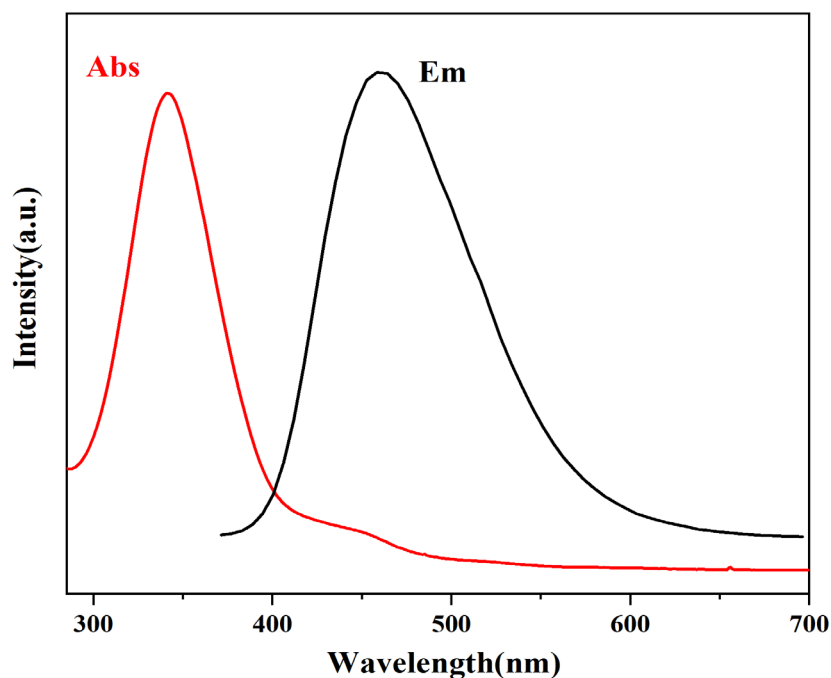


Figure 3.6 The UV-Vis absorption and fluorescence spectra of N-CQDs ( $\lambda_{ex} = 350$  nm)

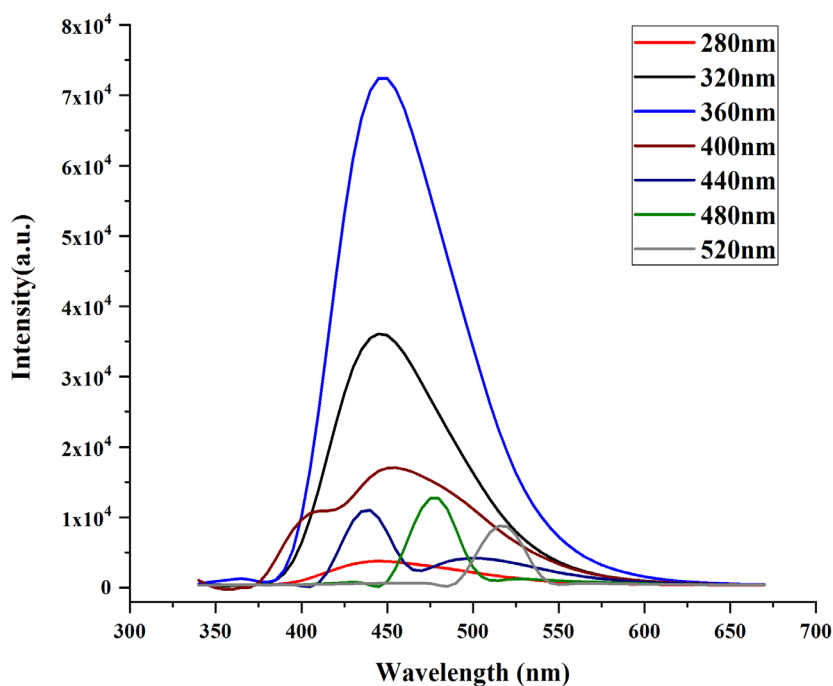


Figure 3.7 Emission spectra of N-CQDs under different excitation wavelengths

To further explore the optical properties of the as-prepared N-CQDs, we carried out a detailed PL study with different excitation wavelengths ranging from 280 to 520 nm (Fig. 3.7). When the  $\lambda_{\text{ex}}$  is larger than 440 nm, the as-prepared N-CQDs exhibit an excitation-dependent PL behavior. More specifically, the emission peak shifted from 440 to 480/520 nm by changing the  $\lambda_{\text{ex}}$  from 440 to 480/520 nm. In contrast, the fluorescence emission peak remained almost unchanged (at 440 nm) for the  $\lambda_{\text{ex}}$  over 280–440 nm and the highest fluorescence intensity appears at  $\lambda_{\text{ex}}$  of 360 nm. According to Song et al (2015), N-CQDs derived from the hydrothermal reaction of CA and EDA are mixtures containing imidazo[1,2-*a*]pyridine-7-carboxylic acid (IPCA), oligomers and carbon cores. IPCA, a bright blue fluorophore, was proven to contribute to the molecular state fluorescence. Carbon cores in N-CQDs include polymer clusters and nanosized ( $< 10$  nm) carbon particles. Carbon core shows excitation-dependent fluorescence behaviors, which is called carbon core state, opposite to the molecular

state. The multi-fluorescence response of the N-CQDs is mainly due to the complex components and multiple fluorescence centers in N-CQDs product. Product fractionation is necessary to produce excitation-independent CQDs.

The influence of pH on the fluorescence of N-CQDs was studied at  $\lambda_{\text{ex}}$  of 350 nm to understand the impact of surface functional groups on the fluorescence of N-CQDs. Fig.3.8 demonstrates the effect of solution pH on the fluorescence emission of N-CQDs. There are no significant variations in both the emission wavelength and emission intensity when the pH of N-CQDs solution changes from pH 4.0 to pH 10.0. However, red shift and fluorescence quenching were observed for N-CQDs under pH 2.0. pH-dependent photoluminescence properties of N-CQDs may be caused by the surface states of the carboxylic ( $-\text{COOH} / -\text{COO}^-$ ) group attached to N-CQDs. At acidic pH, the amount of  $-\text{COOH}$  group on the N-CQDs surface is dominant because of the less probability to form deprotonated carboxylate ( $-\text{COO}^-$ ) group. When the  $-\text{COOH}$  functional group is excited at 350 nm, a nonbonding electron of O in  $\text{C}=\text{O}$  is promoted to the antibonding orbital of  $\text{C}=\text{O}$ . The  $(n, \pi^*)_{\text{CO}}$  band of the  $-\text{COOH}$  group can easily couple with the adjacent  $(n, \sigma^*)$  band of OH according to the Norrish reaction, and cause the single bond to rupture if the  $(n, \sigma^*)$  bond is in a repulsive configuration. Thus, the fluorescence intensity of N-CQDs/ $-\text{COOH}$  will be suppressed by the adjacent bond coupling under pH 2.0 (Dhenadhayalan et al., 2015). In contrast, the  $(n, \pi^*)_{\text{CO}}$  band in the carboxylate ( $-\text{COO}^-$ ) group lacks the diabatic coupling with its adjacent single bond such that no significant suppression of N-CQDs fluorescence is observed under pH 4.0 – 10.0.

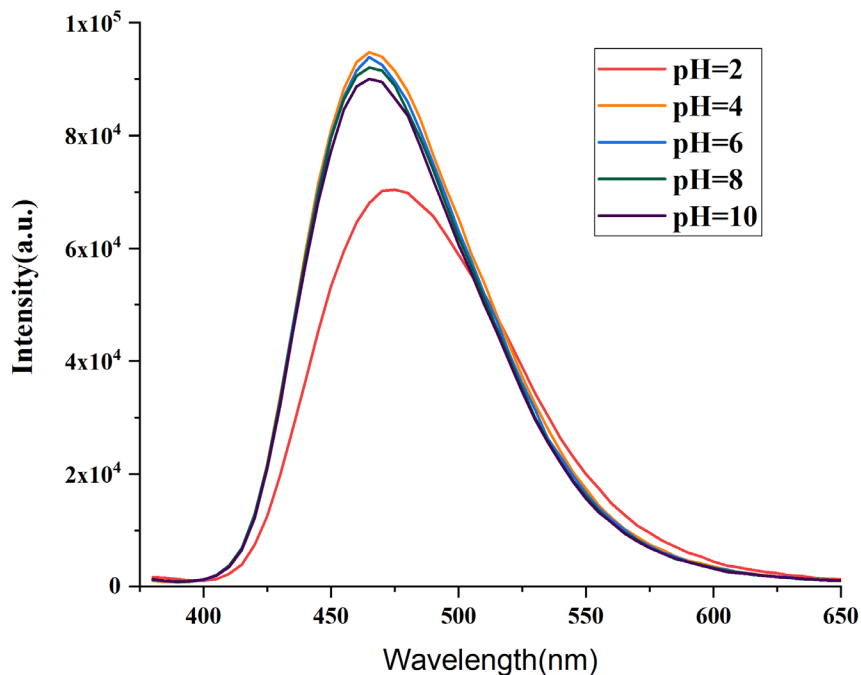


Figure 3.8 The effect of pH on fluorescence spectra of N-CQDs ( $\lambda_{ex} = 350$  nm)

### 3.4 Conclusion

Design of experiments was employed in this study to optimize the hydrothermal synthesis of the N-CQDs from CA and EDA by varying the initial concentration of CA, the molar ratio of EDA to CA, and the reaction temperature. The results from ANOVA analysis reveal that the molar ratio of EDA to CA, and the reaction temperature are the key factors influencing the reaction rate and the reaction products, thus significantly affect the QY of the N-CQDs. The optimum hydrothermal conditions of N-CQDs (QY=51.7%) are initial CA concentration of 0.5 mol/L, EDA to CA molar ratio of 1, and reaction temperature of 180°C. Characterization of N-CQDs by XPS and FTIR confirmed the existence of carbon-core and surface domains of N-CQDs (i.e., the existence of multiple fluorescence centers), which explained the multifluorescence response of N-CQDs under different excitation wavelengths.

## **Chapter 4 CQDs-Incorporated Chitosan Hydrogel Film for Selective Sensing of Hg<sup>2+</sup> Ion**

### **4.1 Introduction**

Environmental contamination by heavy metals has been a serious threat to the ecological system and human health due to their increasing use in domestic, industrial, agricultural and medical applications (Zhao et al., 2015). The non-biodegradable heavy metal ions have been extensively detected in various environmental matrices (water, wastewater, sediments, and biota). Rapid detection of toxic heavy metal ions in water plays an important role in the proper control of water quality and safety. To date, several detection methods, such as atomic absorption spectrometry (AAS), inductively coupled plasma optical emission spectrometry (ICP-OES), and inductively coupled plasma mass spectrometry (ICP-MS) have been widely used for quantitative detection of heavy metal ions with high sensitivity (Kataoka et al., 2015). However, these techniques normally require complicated instrumental settings and pretreatment of water samples, which made them not feasible for on-site detection. There is a huge demand for developing rapid, economical, and highly selective on-site detection of toxic heavy metals.

Advances in fluorescent nanomaterials have paved the way of exploring new tools for optical sensing (Liu et al., 2009; Pan et al., 2015). Recently, carbon quantum dots (CQDs) with superior fluorescence property, particularly obtained from low-cost and abundant biomasses have received great attention as fluorescent probes for the detection of heavy metal ions (Guo et al., 2017). However, “naked” CQDs tend to aggregate in neutral condition, leading to a dramatic decrease in fluorescence intensity (Liu et al., 2019). To stabilize CQDs and improve their performance, immobilization of CQDs

within supramolecular frameworks has been pursued intensively in recent years (Cayuela et al., 2015; Miao et al., 2018; Rizzo et al., 2018; Zhou et al., 2017). CQDs have been incorporated into different polymeric matrices (e.g., poly (methyl acrylate), polyurethane, and polyvinyl alcohol, etc.) to prevent aggregation-induced fluorescence quenching and produce fluorescent materials for practical sensing applications.

Compared to other nanocarriers, hydrogels possess unique physical properties such as hydrophilicity, porosity, tunable cross-linking density, and stability in biological milieu. Therefore, embedding CQDs into polymeric hydrogels is a valuable technique to fabricate fluorescent composite materials with distinct characteristics and unique properties, which endow them with great potential applications as sensors (Gogoi et al., 2015; Ikeda et al., 2011) optical and electrical devices (Jang et al., 2012; Thete et al., 2009), or imaging agents (Li et al., 2019). So far, different assembly methods have been exploited to integrate CQDs into hydrogel networks. Sophisticated variations in structural architectures of composite hydrogel materials are made possible by host–guest interaction (Lu et al., 2018) incorporation of fluorophores into polymer matrices by infusion (Chen & Feng, 2015), self-assembly (Beneduci et al., 2015), and co-assembly of gel hybrids via bioconjugation (Elmalem et al., 2014).

A common fabrication strategy for fluorescent hydrogels is incorporating fluorophore entities (e.g., CQDs) into the hydrogel matrix by weak, non-covalent interactions (Li et al., 2019). Novel chitosan–CQDs nanocomposite hydrogel films were recently prepared based on the electrostatic interaction of the positive charge on chitosan and the negative charge on CQDs (Konwar et al., 2015). The electrostatic interaction rendered the as-prepared chitosan–CQDs films excellent thermal stability, high tensile strength and superior UV-Vis blocking property. Similar method was employed to synthesize CQDs



rooted agarose hydrogel film which can be used as both colorimetric-optical sensor and membrane filter for quintet heavy metal ions (Gogoi et al., 2015). Although simple and easy to scale-up, such non-covalent bonding of CQDs with the gel network may later result in leaching of the fluorescent entities and/or aggregation of CQDs, resulting in loss of luminescence. Further research is needed to investigate the chemical and fluorescence stability of the CQDs-incorporated hydrogels.

Selection of appropriate polymer matrix is not a trivial task for the design of a cost-effective CQDs-based composite hydrogel. Based on the origin of the polymers, the hydrogels thereof are broadly classified into natural and synthetic (Ahmed 2015). Biopolymers in general offers good properties (e.g., nontoxicity, biodegradability and biocompatibility) and are available in abundance (Konwar et al., 2015). Chitosan, a biological cationic polymer composed of randomly distributed  $\beta$ -(1 $\rightarrow$ 4)-linked D-glucosamine and *N*-acetyl-D-glucosamine, has attracted great interest as a carrier for biomedical applications due to abundant sources and low prices. Besides, chitosan can be easily modified or blended with specific molecules to introduce distinct functionalities and/or properties (luminescence, conductivity, mechanical performance, etc) (Barata et al., 2016). Although various chitosan hydrogels or chitosan hydrogel composites have been fabricated as adsorbents, food packing materials, wood dressing materials, drug delivery carriers, few studies refer to the natural biopolymer-based fluorescence sensors for the detection of heavy metal ions. Therefore, incorporating fluorescence CQDs into chitosan hydrogel for constructing an effective fluorescence sensor deserves more research and development efforts.

In this study, a CQDs-based chitosan hydrogel film was fabricated as a fluorescence sensor for a rapid and selective detection of  $\text{Hg}^{2+}$ , one of the most toxic metal ions,

which may cause severe damage to the central nervous system and kidney failure even at a low exposure (Wang et al., 2012). Systematic characterization and optimization of the composite hydrogel film were performed to identify its structural and functional attributes. Quantitative fluorescence measurement of the composite hydrogel in various metal solutions was carried out to evaluate its sensing performance for  $\text{Hg}^{2+}$  ion. Finally, the potential sensing mechanism of  $\text{Hg}^{2+}$  by the composite hydrogel was elucidated with the aid of XPS analysis of the composite hydrogel.

## **4.2 Materials and Methods**

### **4.2.1 Materials**

ACS grade citric acid anhydrous, 99% ethylenediamine, chitosan (85% degree of deacetylation), ACS grade glacial acetic acid, glutaraldehyde (25% aqueous solution), as well as ACS grade nitrate salts ( $\text{Cd}(\text{NO}_3)_2$ ,  $\text{Hg}(\text{NO}_3)_2$ , and  $\text{Pb}(\text{NO}_3)_2$ ) were purchased from Fisher Scientific (Canada). These chemicals were used as received without further purification. All solutions were prepared with deionized water from a Milli-Q water purification system (Millipore Corporation).

### **4.2.2 Synthesis of fluorescent N-CQDs**

N-CQDs were synthesized using the hydrothermal method as described in Chapter 3 of this thesis. To prepare N-CQDs, 3.842 g (0.02 mole) of citric acid was mixed with 1.202g (0.02 mole) of ethylenediamine in a 100 ml Teflon-lined autoclave chamber containing 40.0 ml DI water and heated in an oven at 180 °C for 4 h. After the hydrothermal reaction, membrane filtration and centrifugation of the resultant brown solution were conducted to obtain the N-CQDs suspension. Solid N-CQDs were collected from freeze-drying after a dialysis purification of the N-CQDs product. Solid

N-CQDS were re-dispersed in ethanol-water (1:1 v/v) solution and stored at 4 °C for further use.

#### **4.2.3 Preparation of N-CQDs@GACTS hydrogel film**

In a typical procedure, chitosan (CTS) solution of 1.5% (w/v) was prepared by dissolving 0.15 g of chitosan in 10.0 mL of glacial acetic acid (1% v/v) solution and magnetically stirred at room temperature for 30 min. Crosslinking of chitosan hydrogel was carried out by dropwise addition of 0.25 M glutaraldehyde (GA) to chitosan solution under constant shaking at 50°C for 2 h. After that, 40.0 mg of N-CQDs (from 20.0 g/L ethanol/water solution) were added dropwise to the GA cross-linked chitosan (GACTS) hydrogel to obtain the N-CQDs incorporated chitosan (N-CQDs@GACTS) hydrogel. After vigorous stirring for 15 min and ultrasonication for another 15 min, the as-prepared N-CQDs@GACTS hydrogel was cast on a PVC plate to form thin films, which were then dried overnight at room temperature.

#### **4.2.4 Selective sensing of Hg<sup>2+</sup> ion**

Sensing selectivity of the N-CQDs@GACTS hydrogel was studied by mixing the hydrogel with each metal ion (Cd<sup>2+</sup>, Hg<sup>2+</sup>, and Pb<sup>2+</sup>). Fluorescence emission intensities ( $\lambda_{em} = 450$  nm) of N-CQDs@GACTS hydrogel were measured in the presence (I) and in the absence of (I<sub>0</sub>) interference at the excitation wavelength of 350 nm ( $\lambda_{ex} = 350$  nm). Solutions with the same concentration of each metal ion (100 nM) were prepared for the selectivity measurement.

The detection of Hg<sup>2+</sup> by the N-CQDs@GACTS hydrogel was performed in water solution. 2.5 mL metal solution with different concentrations of Hg<sup>2+</sup> ion (1.0 nM–100.0  $\mu$ M) was added to 0.5 mL N-CQDs@GACTS hydrogel to evaluate the linear

concentration range and the limit of detection. The fluorescence spectra at  $\lambda_{em} = 450$  nm were recorded and all experiments were performed at room temperature.

The fluorescence spectra of the N-CQDs@GACTS hydrogels from different synthetic batches were measured, the optical properties of the hydrogels are of no noticeable difference. This means that the repeatability of the fluorescence spectra is very well. There are no significant variations from different measurements of the same samples for  $Hg^{2+}$  sensing as well.

#### **4.2.5 Characterization**

The N-CQDs@GACTS hydrogel film was characterized by various techniques. The Fourier transform infrared (FTIR) spectra of N-CQDs@GACTS film were measured by a Bruker Tensor II FTIR spectrometer (Bruker, Germany) over a range from 400 to 4000  $cm^{-1}$ . X-ray photoelectron spectroscopy (XPS) measurements of the as-prepared hydrogel film were performed using an XPS - PHI 5000 VPIII (ULPAC-PHI Inc., Japan). A PTI-QuantaMaster spectrofluorometer (Photon Technology International Inc., USA) was used to record the excitation and emission spectra of N-CQDs@GACTS hydrogel before and after metal detection.

### **4.3 Results and Discussion**

#### **4.3.1 Degree of crosslinking for GACTS hydrogel films**

As we all know that the degree of crosslinking will have a significant influence on the physical and chemical properties of hydrogel films. In order to get a GACTS hydrogel film with sufficient mechanical strength, different levels of crosslinking were explored by adding different amounts of GA to CTS solutions. Figure 4.1 shows the as-prepared GACTS hydrogel films with three different levels of crosslinking. The CTS film

without crosslinking is very fragile and with very poor mechanical strength. With the increase in the degree of crosslinking, the color of the hydrogel films becomes darker and the hardness of the films increases accordingly. However, when a high degree (10%) of crosslinking was applied, the elongation or mobility of the hydrogel was lost, and it was very difficult for the thin film to form. Therefore, 5% degree of cross-linking was utilized in the subsequent experiments to fabricate both GACTS and N-CQDs@GACTS hydrogel films.

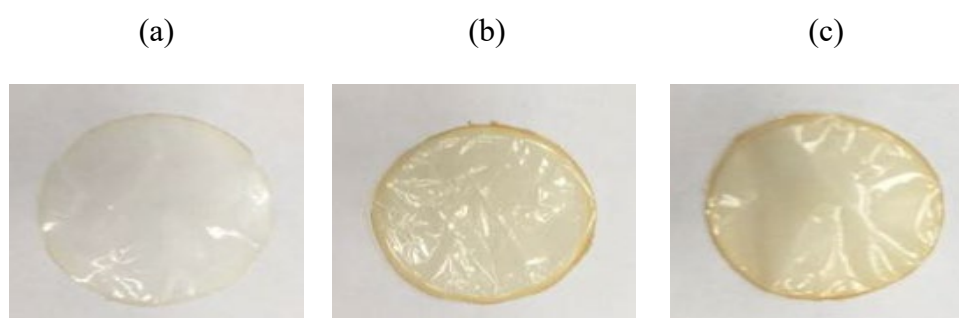


Figure 4.1 GACTS hydrogel films with different degrees of crosslinking: 0%(a); 5%(b); 10%(c)

#### 4.3.2 Characterization of N-CQDs@CTS hydrogel film

FTIR spectra of pure chitosan, GACTS and N-CQDs@GACTS hydrogel films were examined to validate the crosslinking of CTS and potential interactions between N-CQDs and GACTS hydrogel film (Fig. 4.2). As previously reported (Nghah et al., 2008; Zhang et al., 2015), pure chitosan presents the  $-OH$  along with  $-NH$  broad stretching vibration peaks in a range between  $3200-3600\text{ cm}^{-1}$ , the  $-NH$  bending vibration peaks at  $1638.7$  and  $1544.3\text{ cm}^{-1}$ , as well as the  $C-N$  and  $C-O$  stretching vibration peaks at  $1150.4$  and  $1066.1\text{ cm}^{-1}$ , respectively. The effective crosslinking of CTS with GA, which occurred at the amino groups of CTS could be confirmed from the significant peak shifts of the  $-NH$  bending vibration from  $1638.7$  to  $1641.3\text{ cm}^{-1}$  and  $1544.3$  to  $1552.5\text{ cm}^{-1}$ . After incorporating N-CQDs into the GACTS hydrogel, the band peak of

the C–N stretching vibration in the spectrum of N-CQDs@GACTS hydrogel film is shifted to 1151.7  $\text{cm}^{-1}$  from 1150.8  $\text{cm}^{-1}$  due to the coalescence of C–N stretching vibrations of both GACTS and N-CQDs. The IR results of GACTS and N-CQDs@GACTS do not support the formation of any new bonds between N-CQDs and GACTS, which indicates that N-CQDs were embedded into the GACTS matrix mainly through weak hydrogen bond or electrostatic attraction.

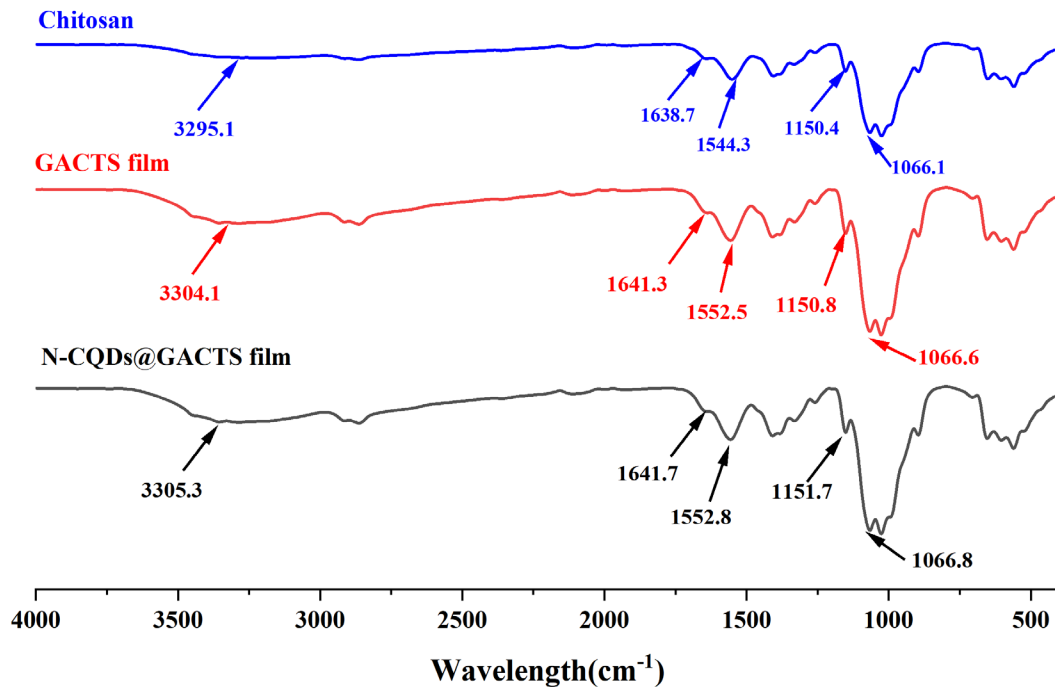


Figure 4.2 FTIR spectra of chitosan, GACTS and N-CQDs@GACTS films

The surface composition and elemental analysis of the N-CQDs@GACTS hydrogel film was characterized by XPS. Figure 4.3 illustrates the XPS survey spectra of N-CQDs@GACTS hydrogel film before and after metal sensing. It should be addressed that binding energies in all the XPS spectra have been recalibrated by shifting C 1s peak to 284.8 eV. The peaks at 284.6, 399.0 and 532.2 eV in the XPS survey spectrum of N-

CQDs@GACTS hydrogel film before  $\text{Hg}^{2+}$  sensing are attributed to C 1s, N 1s, and O 1s, respectively. The peaks at 284.7, 346.5, 399.1, and 532.4 eV in the survey spectrum of hydrogel film after  $\text{Hg}^{2+}$  sensing can be attributed to C 1s, Hg 4d, N 1s, and O 1s, respectively.

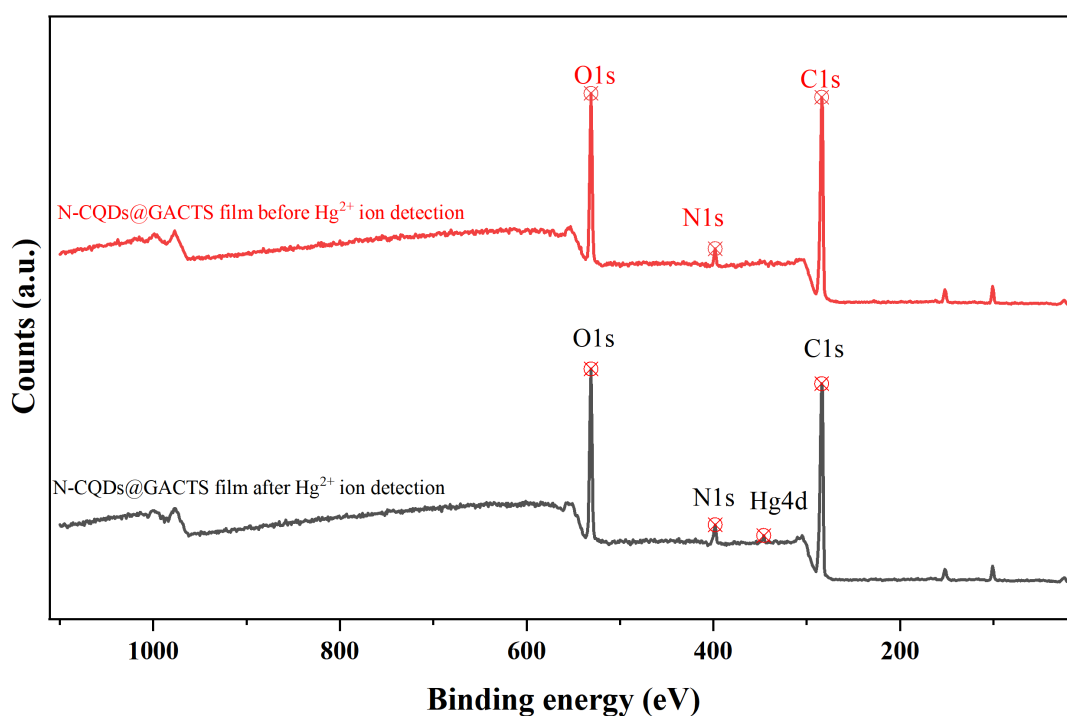


Figure 4.3 XPS survey spectra of N-CQDs@GACTS film before and after  $\text{Hg}^{2+}$  sensing

### 4.3.3 Optical properties of N-CQDs@GACTS film

From Figure 4.4, both GACTS hydrogel and N-CQDs exhibit blue fluorescence emissions (Geng et al., 2015). In order to reveal their contributions to the fluorescence property of the composite hydrogel film, the fluorescence excitation and emission spectra of the GACTS and the N-CQDs@GACTS hydrogel films are compared in Fig. 4.4. As seen from Fig.4.4a, the GACTS film can be excited by wavelengths between 240 and 250 nm. With the excitation wavelength being set at 250 nm, strong fluorescence emission peaks centered at 345 and 450 nm can be clearly observed. From

the spectra of the N-CQDs@GACTS hydrogel film illustrated in Fig 4.4b, the strongest excitation wavelength at 345 nm is observed, whereas its strongest emission wavelength is found to be 450 nm ( $\lambda_{em} = 450$  nm). Compared with the GACTS film, the fluorescence emission intensity of N-CQDs@GACTS hydrogel film is about 25 times stronger, which indicates that the fluorescence property of the composite hydrogel film mainly stems from the N-CQDs.

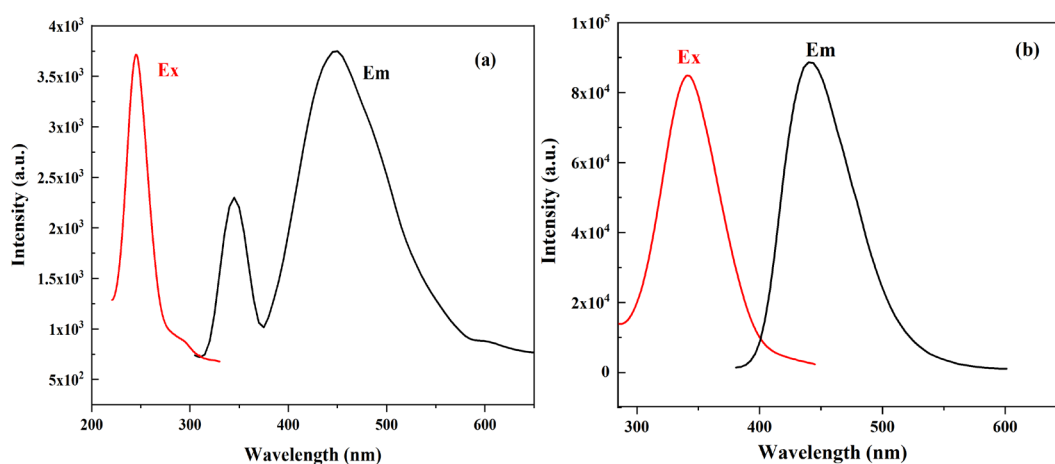


Figure 4.4 The excitation and emission spectra of (a) GACTS film and (b) N-CQDs@GACTS films

#### 4.3.4 Sensing selectivity of N-CQDs@GACTS hydrogel

The sensing selectivity of the as-prepared N-CQDs@GACTS hydrogel towards certain metal ion(s) was studied by mixing N-CQDs@GACTS hydrogel with different ions solutions ( $Cd^{2+}$ ,  $Hg^{2+}$ , and  $Pb^{2+}$ ), each at a concentration of 100.0 nM. As can be witnessed from Fig. 4.5a, the fluorescent N-CQDs@GACTS hydrogel shows remarkable quenching effect on  $Hg^{2+}$  than the other two ions. The fluorescence emission intensity of N-CQDs@GACTS hydrogel was reduced more than 60% after being immersed in the  $Hg^{2+}$  solution. Nonetheless, no significant change in the



fluorescence intensity was observed after the composite hydrogel was immersed in  $\text{Cd}^{2+}$  or  $\text{Pb}^{2+}$  solution.

The images in Fig 4.5b intuitively show that N-CQDs@GACTS hydrogel underwent fluorescence quenching in  $\text{Hg}^{2+}$  solution under 395 nm UV light. Whereas the quenching effect is almost unnoticeable after adding  $\text{Cd}^{2+}$  and  $\text{Pb}^{2+}$  ions into N-CQDs@GACTS hydrogel, which further confirmed the good sensing selectivity of the N-CQDs@GACTS hydrogel.

The excellent selectivity could be attributed to a stronger interaction between the N-CQDs@GACTS hydrogel and  $\text{Hg}^{2+}$  than other metal ions. Among the three divalent metal ions,  $\text{Hg}^{2+}$  has the strongest oxidizing ability and the smallest hydraulic radius and it is therefore more easily combined with polar groups on the surface of N-CQDs@GACTS hydrogel by either chelation or electrostatic attraction (Gao et al., 2019), making  $\text{Hg}^{2+}$  better than  $\text{Cd}^{2+}$  and  $\text{Pb}^{2+}$  for the quenching effect of the fluorescent composite hydrogel.

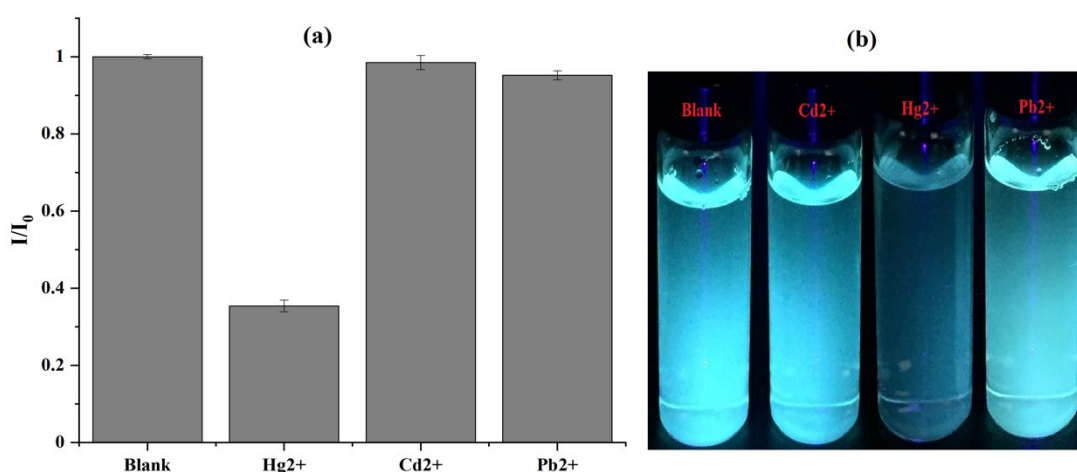


Figure 4.5 The  $I/I_0$  ratio of N-CQDs@GACTS hydrogel in the presence of 100nM different metal ions (a); and images of N-CQDs@GACTS hydrogel in the presence of metal ions under 395nm UV light (b).

### 4.3.5 Sensing of Hg<sup>2+</sup> ions

For a sensitivity study, the fluorescence response of the N-CQDs@GACTS hydrogel to different concentrations of Hg<sup>2+</sup> was investigated and the results were demonstrated in Fig. 4.6a. It can be seen that the fluorescence intensity of the N-CQDs@GACTS hydrogel keeps on decreasing with the increase of Hg<sup>2+</sup> concentration, i.e., the degree of fluorescence quenching increases synchronously with the concentration of Hg<sup>2+</sup>. Moreover, relatively faster decrease in fluorescence intensity at  $\lambda_{em} = 450$  nm is observed with the concentration of the Hg<sup>2+</sup> up to 10.0  $\mu$ M. Whereas, more gradual decrease in fluorescence intensity ( $\lambda_{em} = 450$  nm) is perceived when the concentration of Hg<sup>2+</sup> exceeds 25.0  $\mu$ M. When the quenching effect  $((I_0-I)/I_0)$  data were plotted as a function of Hg<sup>2+</sup> concentration, a very good linear correlation ( $R^2 = 0.997$ ) was obtained within the concentration range of 1.0 ~ 100.0 nM (Fig. 4.6b). Most importantly, a remarkable quenching effect  $((I_0-I)/I_0 = 59\%)$  was still attainable when the concentration of Hg<sup>2+</sup> was reduced to 1.0 nM, which is below the maximum permitted level of Hg<sup>2+</sup> (5.0 nM) in drinking water. All these results clearly indicate that the N-CQDs@GACTS hydrogel is very sensitive in detecting trace amount of Hg<sup>2+</sup> from water solution. Table 4.1 compares the sensing performance of N-CQDs@GACTS hydrogel with those of other CQDs-based optical sensors.

Table 4.1 Comparison of detection performances of CQDs-based composites for Hg<sup>2+</sup>

<b>Fluorescent materials</b>	<b>Lowest detection conc.</b>	<b>References</b>
CQDs@Tb(TFA) <sub>3</sub>	0.55 $\mu$ M	Zou et al., 2020
Eu <sup>3+</sup> /CQDs@MOF-253	6.5 nM	Xu & Yan, 2016
GA cross-linked CTS hydrogel	5.0 nM	Geng et al., 2015
CQDs-PEGDA	4.0 nM	Guo et al., 2017
CQDs-orgaosilane	1.7 nM	Wang et al., 2015
N-CQDS@GACTS hydrogel	1.0 nM	This work

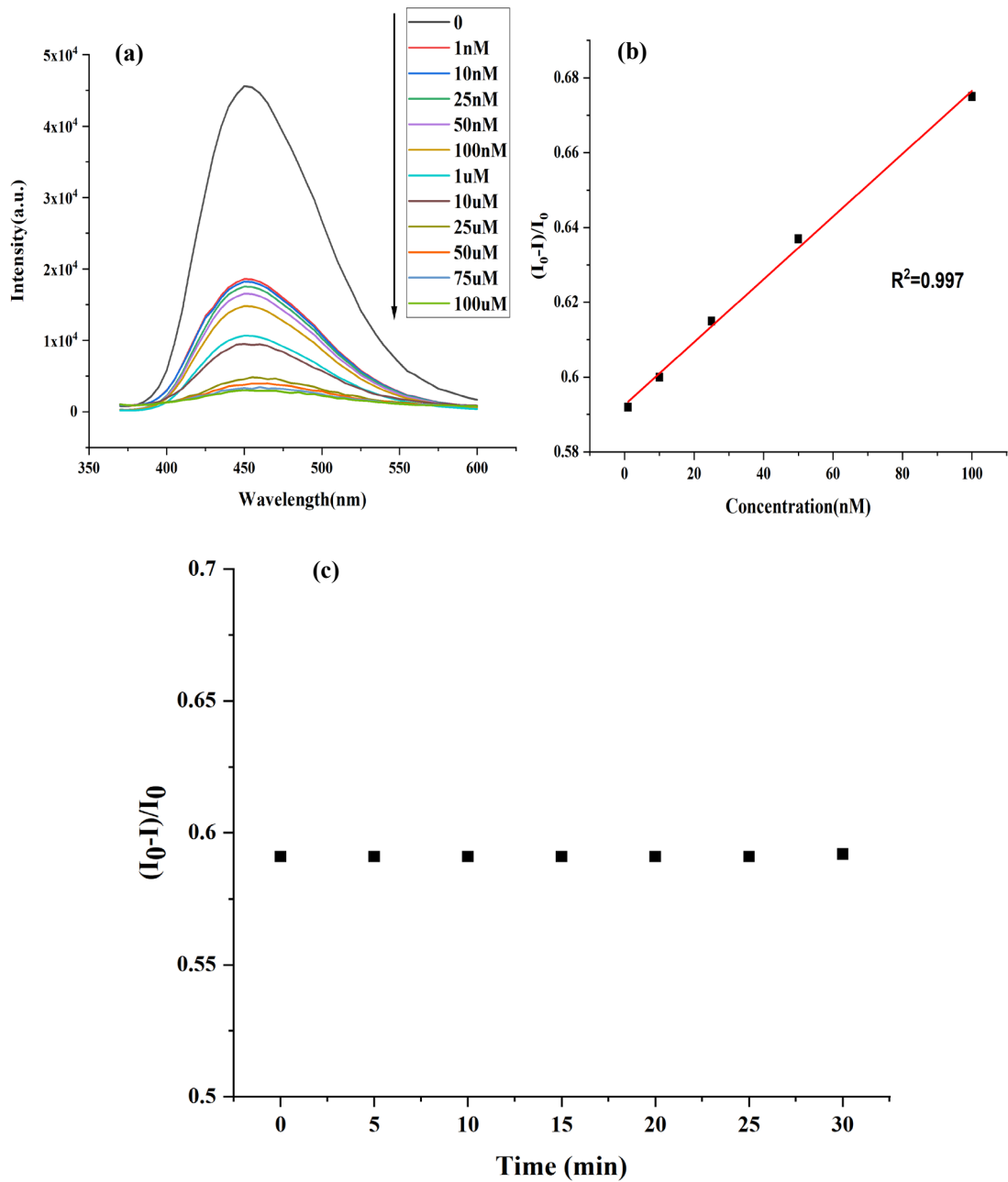


Figure 4.6 The fluorescence intensity spectra of N-CQDs@GACTS hydrogel in the presence of Hg<sup>2+</sup> ion (0~100μM) (a); the fluorescence quenching rates of N-CQDs@GACTS hydrogel under different concentrations of Hg<sup>2+</sup> (b); time-dependent fluorescence intensity of N-CQDs@GACTS hydrogel(c)

The response time for fluorescence quenching is another important parameter to evaluate the fluorescence detection performance of fluorescent probes. Fig. 4.6c shows the time dependent fluorescence intensity ( $\lambda_{em} = 450 \text{ nm}$ ) of the N-CQDs@GACTS

hydrogel quenched with 1 nM  $\text{Hg}^{2+}$  excited at 350 nm. It can be seen that the fluorescence intensity of the N-CQDs@GACTS hydrogel remained almost unchanged after being immersed in the  $\text{Hg}^{2+}$  solution for 30 min, which indicates that the quenching effect of the prepared composite hydrogel film to  $\text{Hg}^{2+}$  is extremely fast and stable. It is believed that the fast mass transfer of  $\text{Hg}^{2+}$  ion in the porous N-CQDs@GACTS hydrogel enables the full utilization of the high binding capacity of chitosan hydrogel for  $\text{Hg}^{2+}$  ions, resulting in the rapid response of fluorescence quenching.

The achieved high sensitivity, rapid response time and linear detection ranges of  $\text{Hg}^{2+}$  by N-CQDs@GACTS hydrogel reveal that the as-prepared composite hydrogel has great potential for practical applications in selectively detecting  $\text{Hg}^{2+}$  from drinking water or wastewater.

#### **4.3.6 Sensing mechanism**

Most of the sensing mechanisms are rooted in non-covalent interactions between the hydrogel network and external stimuli (Ji et al. 2013). Complexation of  $\text{Hg}^{2+}$  with N-CQDS@GACTS hydrogel is the main cause for the fluorescence quenching in our system. The formation of the complex between  $\text{Hg}^{2+}$  with the composite hydrogel through coordination bonds accelerates the extinction of electron/hole non-radiation recombination by effective electron transfer (Liu et al., 2016), resulting in fluorescence quenching of N-CQDs on the surface of N-CQDS@GACTS hydrogel film.

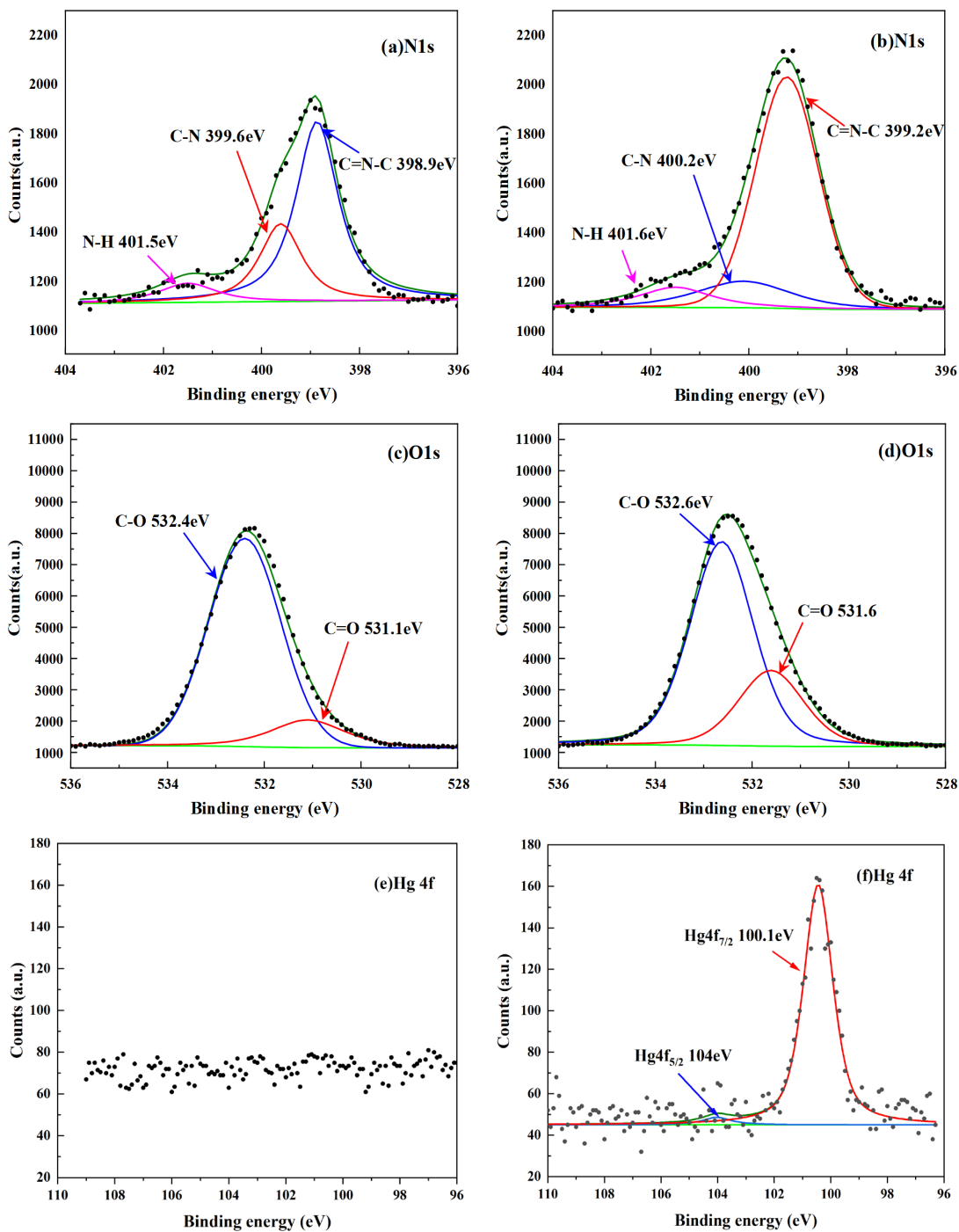


Figure 4.7 High resolution and deconvoluted N 1s (a), O 1s (c) and Hg 4f (e)XPS spectra of N-CQDs@GACTS film before  $\text{Hg}^{2+}$  sensing; N 1s (b), O 1s (d) and Hg 4f (f)XPS spectra of N-CQDs@GACTS film after  $\text{Hg}^{2+}$  sensing.

The interaction between  $\text{Hg}^{2+}$  and CQDS@GACTS hydrogel film was characterized by XPS study. Fig. 4.7 exhibits the high resolution and the deconvoluted XPS spectra of N

1s and O 1s for the N-CQDs@GACTS film before and after  $\text{Hg}^{2+}$  sensing. The three distinct peaks at 398.9, 399.6 and 401.5 eV are visible for N 1s spectrum before metal sensing, which are related to C=N–C (chain group by crosslinking), C–N (pyridinic group in N-CQDs), and N–H (amino group) bonds, respectively. All the three peaks are shifted to higher BE to 339.2, 400.2 and 401.6 eV after  $\text{Hg}^{2+}$  sensing. This result indicates that N in all the three functional groups acts as an electron-donor, helping bind  $\text{Hg}^{2+}$  through electrostatic attraction or chelating. Moreover,  $\text{Hg}^{2+}$  ions are also complexed with O-containing groups (e.g., –OH and –COOH) on N-CQDs@GACTS surface through coordination bonds. This is proved by the peak shifts of O 1s from 531.1(C=O bond) to 531.6 eV and 532.4 (C–O bond) to 532.6 eV. The high-resolution peaks of Hg 4f at BE of 100.1 and 104.0 eV in Fig. 6f confirm the formation of complexes between  $\text{Hg}^{2+}$  and N-CQDs@GACTS hydrogel, which provokes an effective electron transfer for the fluorescence quenching of the N-CQDs@GACTS hydrogel.

#### 4.4 Conclusion

A novel N-CQDs@GACTS hydrogel film was prepared in this study and was used as an optical sensor to detect traces amount of heavy metal ions from water solution. FTIR and XPS analyses of the N-CQDs@GACTS hydrogel film indicate that N-CQDS were embedded into the cross-linked hydrogel matrix by weak hydrogen bond and/or electrostatic attraction. The resultant composite hydrogel exhibited extremely high sensitivity, superior selectively, rapid response and linear detection range of  $\text{Hg}^{2+}$  in aqueous media. The porous structure of the N-CQDs@GACTS hydrogel is believed to render a fast mass transfer of  $\text{Hg}^{2+}$  onto the hydrogel surface. The high oxidizing ability and strong chelating power of  $\text{Hg}^{2+}$  make it readily bind to polar functional groups on

N-CQDs@GACTS hydrogel, resulting the formation of new complexes through coordination bonds. The high resolution XPS results of N 1s and O 1s support the formation of complexes between  $\text{Hg}^{2+}$  ions and the N-CQDs@GACTS hydrogel film, which provokes an effective electron transfer for the fluorescence quenching of the N-CQDs@GACTS hydrogel.

The N-CQDs@GACTS hydrogel as an optical sensor demonstrates enhanced practicality in terms of response, sensitivity, selectivity, and economical pricing. It has great potential for practical applications in selectively detecting  $\text{Hg}^{2+}$  from either drinking water or wastewater.

## Chapter 5 Conclusion and Recommendation

### 5.1 Summary

In this study, the N-CQDs was synthesized from citric acid and ethylenediamine through the hydrothermal method. The prepared N-CQDs possess bright blue light under UV light. By applying the design of experiment (DOE) method and statistical analysis, optimal preparation conditions were determined for N-CQDs. The ANOVA results indicated that the molar ratio of EDA to CA, the reaction temperature, and the interaction between these two factors are the important factors affecting the QY of N-CQDs. The optimal reaction conditions are initial CA concentration of 0.5 mol/L, EDA to CA molar ratio of 1, and the reaction temperature of 180°C based on the 3D surface figure. The excitation-dependent fluorescence response of the N-CQDs is due to the heterogeneity of the resultant N-CQDs product.

To stabilize the N-CQDs and improve their performance on the sensing of heavy metals, the N-CQDs-based glutaraldehyde-crosslinked chitosan hydrogel film was synthesized as a fluorescence sensor. The experimental results showed that N-CQDs@GACTS hydrogel film is highly selective and sensitive to  $\text{Hg}^{2+}$  ion compared to  $\text{Cd}^{2+}$  and  $\text{Pb}^{2+}$  ions. The potential sensing mechanism was further studied using the XPS analysis of the hydrogel film, which confirmed the complexation of  $\text{Hg}^{2+}$  with the hydrogel. Complexation of  $\text{Hg}^{2+}$  with N-CQDs@GACTS hydrogel is believed to be the main cause for the fluorescence quenching of the N-CQDs@GACTS hydrogel film.

In summary, one of the achievements of this study is the synthesis of nitrogen-doped carbon dots and the optimization of the reaction conditions such as the amount of the carbon, nitrogen precursor, and the reaction temperature. The other significant



achievement is the sensing of  $\text{Hg}^{2+}$  by the N-CQDs@GACTS hydrogel and the possible mechanisms of the selective sensing process based on the XPS results.

## 5.2 Recommendations for future work

In this study, a further step of purification is not applied in the synthesis process of N-CQDs, which results in the excitation-dependent fluorescence behaviors of N-CQDs. Besides, the effect of reaction time is not considered when we applied the DOE method to the optimization as it was fixed at four hours in this study. The interaction of time and temperature may also have a more significant impact on the fluorescence yield of N-CQDs. A high fluorescence yield may be achieved by adjusting the reaction time and reaction temperature.

From the sensing experiments of the N-CQDs@GACTS hydrogel film perspective, there are also have some limitations of the heavy metal sensing process. The currently metal detection experiment only focuses on three metal ions ( $\text{Hg}^{2+}$ ,  $\text{Cd}^{2+}$  and  $\text{Pb}^{2+}$ ). In actual sensing applications, the industrial wastewater or pollutants may contain several or more different metal ions. Therefore, whether the presence of multiple ions has an effect on the detection of  $\text{Hg}^{2+}$  ion needs further examination.

Based on the above discussion, some recommendations for future work are described as following:

- (1) In future research, a more stringent purification step can be used to synthesize excitation-independent N-CQDs product. Therefore, the aimed CQDs with average size can be achieved.
- (2) The extra factor like reaction time can be added to the DOE design to investigate its effect on the QY of N-CQDs.

- (3) In subsequent research, other heavy metal ions such as nickel ions, cobalt ions, etc., can be studied in future work.
- (4) Multi-metal mixing sensing experiments can be arranged to study whether it has a synergistic or antagonistic effect on detecting  $\text{Hg}^{2+}$  ions.

## References

- Abd Rani, U., Ng, L. Y., Ng, C. Y., & Mahmoudi, E. (2020). A review of carbon quantum dots and their applications in wastewater treatment. *Advances in Colloid and Interface Science*, 102124.
- Ahmed, E. M. (2015). Hydrogel: Preparation, characterization, and applications: A review. *Journal of advanced research*, 6(2), 105-121.
- Ananthanarayanan, Arundithi, Wang, Yue, Routh, Parimal, Sk, Mahasin Alam, Than, Aung, Lin, Ming, Zhang, Jie, Chen, Jie, Sun, Handong, and Chen, Peng (2015). Nitrogen and phosphorus co-doped graphene quantum dots: Synthesis from adenosine triphosphate, optical properties, and cellular imaging. *Nanoscale*, 7(17), 8159-8165.
- Arora, N., & Sharma, N. N. (2014). Arc discharge synthesis of carbon nanotubes: Comprehensive review. *Diamond and related materials*, 50, 135-150.
- Baker, Sheila N, & Baker, Gary A. (2010). Luminescent Carbon Nanodots: Emergent Nanolights. *Angewandte Chemie (International Ed.)*, 49(38), 6726-6744.
- Barata, J.F., Pinto, R.J., Vaz Serra, V.I., Silvestre, A.J., Trindade, T., Neves, M.G.P., Cavaleiro, J.A., Daina, S., Sadocco, P. and Freire, C.S. (2016). Fluorescent bioactive corrole grafted-chitosan films. *Biomacromolecules*, 17(4), 1395-1403.
- Beneduci, A., Cospito, S., Deda, M. L., & Chidichimo, G. (2015). Highly fluorescent thienoviologen-based polymer gels for single layer electrofluorochromic devices. *Advanced Functional Materials*, 25(8), 1240-1247.
- Bhunias, S. K., Nandi, S., Shikler, R., & Jelinek, R. (2016). Tuneable light-emitting carbon-dot/polymer flexible films prepared through one-pot synthesis. *Nanoscale*, 8(6), 3400-3406.
- Bourlinos, Athanasios B, Zbořil, Radek, Petr, Jan, Bakandritsos, Aristides, Krysmann, Marta, & Giannelis, Emmanuel P. (2012). Luminescent Surface Quaternized Carbon Dots. *Chemistry of Materials*, 24(1), 6-8.
- Cao, L., Wang, X., Meziani, M.J., Lu, F., Wang, H., Luo, P.G., Lin, Y., Harruff, B.A., Veca, L.M., Murray, D. and Xie, S.Y. (2007). Carbon dots for multiphoton bioimaging. *Journal of the American Chemical Society*, 129(37), 11318-11319.
- Cayuela, A., Kennedy, S. R., Soriano, M. L., Jones, C. D., Valcárcel, M., & Steed, J. W. (2015). Fluorescent carbon dot–molecular salt hydrogels. *Chemical science*, 6(11), 6139-6146.

- Chandra, Sourov, Patra, Prasun, Pathan, Shaheen H, Roy, Shuvrodeb, Mitra, Shouvik, Layek, Animesh, Bhar, Radhaballabh, Pramanik, Panchanan, and Goswami, Arunava. (2013) Luminescent S-doped carbon dots: an emergent architecture for multimodal applications. *J Mater Chem B* 1(18):2375–2382
- Chen, B. B., Liu, M. L., Li, C. M., & Huang, C. Z. (2019). Fluorescent carbon dots functionalization. *Advances in Colloid and Interface Science*, 270, 165-190.
- Chen, B., & Feng, J. (2015). White-Light-Emitting Polymer Composite Film Based on Carbon Dots and Lanthanide Complexes. *The Journal of Physical Chemistry C*, 119(14), 7865-7872.
- Chu, K. W., Lee, S. L., Chang, C. J., & Liu, L. (2019). Recent progress of carbon dot precursors and photocatalysis applications. *Polymers*, 11(4), 689.
- Ciftja, O. (2012). Quantum dots applications, synthesis and characterization (Nanotechnology science and technology series). *Hauppauge, N.Y.: Nova Science*.
- Dang, H., Huang, L. K., Zhang, Y., Wang, C. F., & Chen, S. (2016). Large-scale ultrasonic fabrication of white fluorescent carbon dots. *Industrial & Engineering Chemistry Research*, 55(18), 5335-5341.
- de Medeiros, T. V., Manioudakis, J., Noun, F., Macairan, J. R., Victoria, F., & Naccache, R. (2019). Microwave-assisted synthesis of carbon dots and their applications. *Journal of Materials Chemistry C*, 7(24), 7175-7195.
- Devi, Pooja, Kaur, Gurvinder, Thakur, Anupma, Kaur, Navneet, Grewal, Anita, & Kumar, Praveen. (2017). Waste derivitized blue luminescent carbon quantum dots for selenite sensing in water. *Talanta (Oxford)*, 170, 49-55.
- Dhenadhayalan, N., Lin, K. C., & Saleh, T. A. (2020). Recent advances in functionalized carbon dots toward the design of efficient materials for sensing and catalysis applications. *Small*, 16(1), 1905767.
- Dhenadhayalan, N., Lin, K., Suresh, R., & Ramamurthy, P. (2016). Unravelling the Multiple Emissive States in Citric-Acid-Derived Carbon Dots. *The Journal of Physical Chemistry C*, 120(2), 1252-1261.
- Ding, H., Wei, J., Zhong, N., Gao, Q., & Xiong, H. (2017). Highly Efficient Red-Emitting Carbon Dots with Gram-Scale Yield for Bioimaging. *Langmuir: The ACS Journal of Surfaces and Colloids*, 33(44), 12635-12642.
- Ding, Hui, & Xiong, Huan-Ming. (2015). Exploring the blue luminescence origin of nitrogen-doped carbon dots by controlling the water amount in synthesis. Electronic supplementary information (ESI) available. See DOI: 10.1039/c5ra11796h. 5(82), 66528-66533.

- Ding, Hui, Wei, Ji-Shi, & Xiong, Huan-Ming. (2014). Nitrogen and sulfur co-doped carbon dots with strong blue luminescence. *Nanoscale*, 6(22), 13817-13823.
- Do, Sungan, Kwon, Woosung, & Rhee, Shi-Woo. (2014). Soft-template synthesis of nitrogen-doped carbon nanodots: Tunable visible-light photoluminescence and phosphor-based light-emitting diodes. *Journal of Materials Chemistry. C, Materials for Optical and Electronic Devices*, 2(21), 4221.
- Dong, Y., Pang, H., Yang, H. B., Guo, C., Shao, J., Chi, Y., & Yu, T. (2013). Carbon-based dots co-doped with nitrogen and sulfur for high quantum yield and excitation-independent emission. *Angewandte Chemie International Edition*, 52(30), 7800-7804.
- Dong, Yongqiang, Shao, Jingwei, Chen, Congqiang, Li, Hao, Wang, Ruixue, Chi, Yuwu, Lin, Xiaomei, and Chen, Guonan. (2012). Blue Luminescent Graphene Quantum Dots and Graphene Oxide Prepared by Tuning the Carbonization Degree of Citric Acid. *Carbon (New York)* 50.12: 4738-743.
- Du, J., Xu, N., Fan, J., Sun, W., & Peng, X. (2019). Carbon dots for in vivo bioimaging and theranostics. *Small*, 15(32), 1805087.
- Eda, G., Lin, Y.Y., Mattevi, C., Yamaguchi, H., Chen, H.A., Chen, I.S., Chen, C.W. and Chhowalla, M. (2010). Blue photoluminescence from chemically derived graphene oxide. *Advanced materials*, 22(4), 505-509.
- Elmalem, E., Biedermann, F., Scherer, M. R., Koutsioubas, A., Toprakcioglu, C., Biffi, G., & Huck, W. T. (2014). Mechanically strong, fluorescent hydrogels from zwitterionic, fully  $\pi$ -conjugated polymers. *Chemical communications*, 50(64), 8930-8933.
- Fang, Youxing, Guo, Shaojun, Li, Dan, Zhu, Chengzhou, Ren, Wen, Dong, Shaojun, & Wang, Erkang. (2012). Easy Synthesis and Imaging Applications of Cross-Linked Green Fluorescent Hollow Carbon Nanoparticles. *ACS Nano*, 6(1), 400-409.
- Gao, W., Zhou, Y., Xu, C., Guo, M., Qi, Z., Peng, X., & Gao, B. (2019). Bright hydrophilic and organophilic fluorescence carbon dots: One-pot fabrication and multi-functional applications at visualized Au<sup>3+</sup> detection in cell and white light-emitting devices. *Sensors and Actuators B: Chemical*, 281, 905-911.
- Gao, X., Du, C., Zhuang, Z., & Chen, W. (2016). Carbon quantum dot-based nanoprobe for metal ion detection. *Journal of Materials Chemistry C*, 4(29), 6927-6945.

- Gao, X., Li, M., Zhao, Y., & Zhang, Y. (2019). Mechanistic study of selective adsorption of Hg<sup>2+</sup> ion by porous alginate beads. *Chemical Engineering Journal*, 378, 122096.
- Gao, Zhi-hao, Lin, Zheng-zhong, Chen, Xiao-mei, Zhong, Hui-ping, & Huang, Zhi-yong. (2016). A fluorescent probe based on N-doped carbon dots for highly sensitive detection of Hg<sup>2+</sup> in aqueous solutions. *Analytical Methods*, 8(10), 2297-2304.
- Garg, Krishan Kishor, & Prasad, Basheshwer. (2016). Development of Box Behnken design for treatment of terephthalic acid wastewater by electrocoagulation process: Optimization of process and analysis of sludge. *Journal of Environmental Chemical Engineering*, 4(1), 178-190.
- Ge, J., Jia, Q., Liu, W., Guo, L., Liu, Q., Lan, M., Zhang, H., Meng, X. and Wang, P. (2015). Red-emissive carbon dots for fluorescent, photoacoustic, and thermal theranostics in living mice. *Advanced Materials*, 27(28), 4169-4177.
- Ge, J., Jia, Q., Liu, W., Lan, M., Zhou, B., Guo, L., Zhou, H., Zhang, H., Wang, Y., Gu, Y. and Meng, X. (2016). Carbon dots with intrinsic theranostic properties for bioimaging, red-light-triggered photodynamic/photothermal simultaneous therapy in vitro and in vivo. *Advanced healthcare materials*, 5(6), 665-675.
- Geng, Z., Zhang, H., Xiong, Q., Zhang, Y., Zhao, H., & Wang, G. (2015). A fluorescent chitosan hydrogel detection platform for the sensitive and selective determination of trace mercury (II) in water. *Journal of Materials Chemistry A*, 3(38), 19455-19460.
- Gogoi, N., Barooah, M., Majumdar, G., & Chowdhury, D. (2015). Carbon dots rooted agarose hydrogel hybrid platform for optical detection and separation of heavy metal ions. *ACS applied materials & interfaces*, 7(5), 3058-3067.
- Guan, W., Gu, W., Ye, L., Guo, C., Su, S., Xu, P., & Xue, M. (2014). Microwave-assisted polyol synthesis of carbon nitride dots from folic acid for cell imaging. *International journal of nanomedicine*, 9, 5071.
- Guo, J., Zhou, M., & Yang, C. (2017). Fluorescent hydrogel waveguide for on-site detection of heavy metal ions. *Scientific reports*, 7(1), 1-8.
- Guo, Yongming, Cao, Fengpu, & Li, Yabo. (2018). Solid phase synthesis of nitrogen and phosphor co-doped carbon quantum dots for sensing Fe<sup>3+</sup> and the enhanced photocatalytic degradation of dyes. *Sensors and Actuators. B, Chemical*, 255, 1105-1111.

- Hao, Juan, Liu, Fenfen, Liu, Nan, Zeng, Mulang, Song, Yonghai, & Wang, Li. (2017). Ratiometric fluorescent detection of Cu<sup>2+</sup> with carbon dots chelated Eu-based metal-organic frameworks. *Sensors and Actuators. B, Chemical*, 245, 641-647.
- He, Jiangling, Zhang, Haoran, Zou, Jinliang, Liu, Yingliang, Zhuang, Jianle, Xiao, Yong, & Lei, Bingfu. (2016). Carbon dots-based fluorescent probe for “off-on” sensing of Hg(II) and I. *Biosensors & Bioelectronics*, 79, 531-535.
- Holá, Kateřina, Sudolská, Mária, Kalytchuk, Sergii, Nachtigallová, Dana, Rogach, Andrey L, Otyepka, Michal, & Zbořil, Radek. (2017). Graphitic Nitrogen Triggers Red Fluorescence in Carbon Dots. *ACS Nano*, 11(12), 12402-12410.
- Hsu, Pin-Che, & Chang, Huan-Tsung. (2012). Synthesis of high-quality carbon nanodots from hydrophilic compounds: Role of functional groups. *Chemical Communications (Cambridge, England)*, 48(33), 3984-3986.
- Hu, C., Li, M., Qiu, J., & Sun, Y. P. (2019). Design and fabrication of carbon dots for energy conversion and storage. *Chemical Society Reviews*, 48(8), 2315-2337.
- Hu, Q., Paau, M.C., Zhang, Y., Gong, X., Zhang, L., Lu, D., Liu, Y., Liu, Q., Yao, J. and Choi, M.M. (2014). Green synthesis of fluorescent nitrogen/sulfur-doped carbon dots and investigation of their properties by HPLC coupled with mass spectrometry. *RSC Advances*, 4(35), 18065-18073.
- Hu, Shengliang, Liu, Jun, Yang, Jinlong, Wang, Yanzhong, & Cao, Shirui. (2011). Laser synthesis and size tailor of carbon quantum dots. *Journal of Nanoparticle Research: An Interdisciplinary Forum for Nanoscale Science and Technology*, 13(12), 7247-7252.
- Hu, Y., Yang, J., Tian, J., Jia, L., & Yu, J. S. (2014). Waste frying oil as a precursor for one-step synthesis of sulfur-doped carbon dots with pH-sensitive photoluminescence. *Carbon*, 77, 775-782.
- Huang, Qitong, Li, Qian, Chen, Yuanfang, Tong, Lili, Lin, Xiaofeng, Zhu, Jieji, & Tong, Qingxiao. (2018). High quantum yield nitrogen-doped carbon dots: Green synthesis and application as “off-on” fluorescent sensors for the determination of Fe<sup>3+</sup> and adenosine triphosphate in biological samples. *Sensors and Actuators. B, Chemical*, 276, 82-88.
- Ikeda, M., Yoshii, T., Matsui, T., Tanida, T., Komatsu, H., & Hamachi, I. (2011). Montmorillonite–supramolecular hydrogel hybrid for fluorocolorimetric sensing of polyamines. *Journal of the American Chemical Society*, 133(6), 1670-1673.
- Jahan, Shanaz, Mansoor, Farrukh, Naz, Shagufta, Lei, Jianping, & Kanwal, Shamsa. (2013). Oxidative Synthesis of Highly Fluorescent Boron/Nitrogen Co-Doped

- Carbon Nanodots Enabling Detection of Photosensitizer and Carcinogenic Dye. *Analytical Chemistry (Washington)*, 85(21), 10232-10239.
- Jaiswal, A., Ghosh, S. S., & Chattopadhyay, A. (2012). Quantum dot impregnated-chitosan film for heavy metal ion sensing and removal. *Langmuir*, 28(44), 15687-15696.
- Jang, E., Kim, S., & Koh, W. G. (2012). Microfluidic bioassay system based on microarrays of hydrogel sensing elements entrapping quantum dot-enzyme conjugates. *Biosensors and Bioelectronics*, 31(1), 529-536.
- Ji, X., Yao, Y., Li, J., Yan, X., & Huang, F. (2013). A supramolecular cross-linked conjugated polymer network for multiple fluorescent sensing. *Journal of the American Chemical Society*, 135(1), 74-77.
- Jia, Q., Ge, J., Liu, W., Liu, S., Niu, G., Guo, L., Zhang, H. and Wang, P. (2016). Gold nanorod@silica-carbon dots as multifunctional phototheranostics for fluorescence and photoacoustic imaging-guided synergistic photodynamic/photothermal therapy. *Nanoscale*, 8(26), 13067-13077.
- Jia, Q., Zhao, Z., Liang, K., Nan, F., Li, Y., Wang, J., Ge, J. and Wang, P. (2020). Recent advances and prospects of carbon dots in cancer nanotheranostics. *Materials Chemistry Frontiers*, 4(2), 449-471.
- Jiang, K., Sun, S., Zhang, L., Lu, Y., Wu, A., Cai, C., & Lin, H. (2015). Red, Green, and Blue Luminescence by Carbon Dots: Full-Color Emission Tuning and Multicolor Cellular Imaging. *Angewandte Chemie International Edition*, 54(18), 5360-5363.
- Jing, S., Zhao, Y., Sun, R. C., Zhong, L., & Peng, X. (2019). Facile and high-yield synthesis of carbon quantum dots from biomass-derived carbons at mild condition. *ACS Sustainable Chemistry & Engineering*, 7(8), 7833-7843.
- Kabuk, Harun Akif, İlhan, Fatih, Avsar, Yasar, Kurt, Ugur, Apaydin, Omer, & Gonullu, Mustafa T. (2014). Investigation of Leachate Treatment with Electrocoagulation and Optimization by Response Surface Methodology. *Clean: Soil, Air, Water*, 42(5), 571-577.
- Kang, Z., & Lee, S. T. (2019). Carbon dots: advances in nanocarbon applications. *Nanoscale*, 11(41), 19214-19224.
- Karami, C., Taher, M. A., & Shahlaei, M. (2020). A simple method for determination of mercury (II) ions by PNBS-doped carbon dots as a fluorescent probe. *Journal of Materials Science: Materials in Electronics*, 1-9.



- Kasprzyk, Wiktor, Świergosz, Tomasz, Bednarz, Szczepan, Walas, Karolina, Bashmakova, Natalia V, & Bogdał, Dariusz. (2018). Luminescence phenomena of carbon dots derived from citric acid and urea – a molecular insight. *Nanoscale*, 10(29), 13889-13894.
- Kataoka, Y., Watanabe, T., Hayashi, T., Teshima, R., & Matsuda, R. (2015). Development of ICP-OES, ICP-MS and GF-AAS methods for simultaneous quantification of lead, total arsenic and cadmium in soft drinks. *Shokuhin eiseigaku zasshi. Journal of the Food Hygienic Society of Japan*, 56(3), 88-95.
- Ke, J., Li, X., Zhao, Q., Liu, B., Liu, S., & Wang, S. (2017). Upconversion carbon quantum dots as visible light responsive component for efficient enhancement of photocatalytic performance. *Journal of colloid and interface science*, 496, 425-433.
- Kim, Sunghu, Yoo, Byung-Kuk, Choi, Yuri, Kim, Byeong-Su, & Kwon, Oh-Hoon. (2018). Time-resolved spectroscopy of the ensembled photoluminescence of nitrogen- and boron/nitrogen-doped carbon dots. *Physical Chemistry Chemical Physics*, 20(17), 11673-11681.
- Ko, H. Y., Chang, Y. W., Paramasivam, G., Jeong, M. S., Cho, S., & Kim, S. (2013). In vivo imaging of tumour bearing near-infrared fluorescence-emitting carbon nanodots derived from tire soot. *Chemical Communications*, 49(87), 10290-10292.
- Konwar, A., Gogoi, N., Majumdar, G., & Chowdhury, D. (2015). Green chitosan–carbon dots nanocomposite hydrogel film with superior properties. *Carbohydrate polymers*, 115, 238-245.
- Kumar, Amit, Chowdhuri, Angshuman Ray, Laha, Dipranjan, Mahto, Triveni Kumar, Karmakar, Parimal, & Sahu, Sumanta Kumar. (2017). Green synthesis of carbon dots from *Ocimum sanctum* for effective fluorescent sensing of Pb<sup>2+</sup> ions and live cell imaging. *Sensors and Actuators. B, Chemical*, 242, 679-686.
- Lai, C. W., Hsiao, Y. H., Peng, Y. K., & Chou, P. T. (2012). Facile synthesis of highly emissive carbon dots from pyrolysis of glycerol; gram scale production of carbon dots/mSiO<sub>2</sub> for cell imaging and drug release. *Journal of Materials Chemistry*, 22(29), 14403-14409.
- Lakowicz, J. R. (Ed.). (2013). Principles of fluorescence spectroscopy. *Springer science & business media*.
- Lan, M., Zhao, S., Zhang, Z., Yan, L., Guo, L., Niu, G., Zhang, J., Zhao, J., Zhang, H., Wang, P. and Zhu, G. (2017). Two-photon-excited near-infrared emissive carbon dots as multifunctional agents for fluorescence imaging and photothermal therapy. *Nano research*, 10(9), 3113-3123.

- Li, D., Jing, P., Sun, L., An, Y., Shan, X., Lu, X., Zhou, D., Han, D., Shen, D., Zhai, Y. and Qu, S. (2018). Near-infrared excitation/emission and multiphoton-induced fluorescence of carbon dots. *Advanced materials*, 30(13), 1705913.
- Li, Fan, Liu, Changjun, Yang, Jian, Wang, Zheng, Liu, Wenguang, & Tian, Feng. (2013). Mg/N double doping strategy to fabricate extremely high luminescent carbon dots for bioimaging. *RSC Advances*, 4(7), 3201-3205.
- Li, G.; Wang, F.; Liu, P.; Chen, Z.; Lei, P.; Xu, Z.; Li, Z.; Ding, Y.; Zhang, S.; Yang, M. (2018). Polymer dots grafted TiO<sub>2</sub> nanohybrids as high performance visible light photocatalysts. *Chemosphere*, 197, 526–534.
- Li, H., He, X., Kang, Z., Huang, H., Liu, Y., Liu, J., Lian, S., Tsang, C.H.A., Yang, X. and Lee, S.T. (2010). Water-soluble fluorescent carbon quantum dots and photocatalyst design. *Angewandte Chemie*, 122(26), 4532-4536.
- Li, H., He, X., Liu, Y., Yu, H., Kang, Z., & Lee, S. T. (2011). Synthesis of fluorescent carbon nanoparticles directly from active carbon via a one-step ultrasonic treatment. *Materials Research Bulletin*, 46(1), 147-151.
- Li, Shuhua, Li, Yunchao, Cao, Jun, Zhu, Jia, Fan, Louzhen, & Li, Xiaohong. (2014). Sulfur-Doped Graphene Quantum Dots as a Novel Fluorescent Probe for Highly Selective and Sensitive Detection of Fe<sup>3+</sup>. *Analytical Chemistry (Washington)*, 86(20), 10201-10207.
- Li, Wenbin, Yue, Zhao, Wang, Cheng, Zhang, Wei, & Liu, Guohua. (2013). An absolutely green approach to fabricate carbon nanodots from soya bean grounds. *RSC Advances*, 3(43), 20662.
- Li, Y., Bai, G., Zeng, S., & Hao, J. (2019). Theranostic carbon dots with innovative NIR-II emission for in vivo renal-excreted optical imaging and photothermal therapy. *ACS applied materials & interfaces*, 11(5), 4737-4744.
- Li, Y., Young, D. J., & Loh, X. J. (2019). Fluorescent gels: a review of synthesis, properties, applications and challenges. *Materials Chemistry Frontiers*, 3(8), 1489-1502.
- Li, Y., Zhao, Y., Cheng, H., Hu, Y., Shi, G., Dai, L., & Qu, L. (2012). Nitrogen-doped graphene quantum dots with oxygen-rich functional groups. *Journal of the American Chemical Society*, 134(1), 15-18.
- Li, Y., Zhao, Y., Cheng, H., Hu, Y., Shi, G., Dai, L., & Qu, L. (2012). Nitrogen-doped graphene quantum dots with oxygen-rich functional groups. *Journal of the American Chemical Society*, 134(1), 15-18.

- Li, Yi-Kun, Yang, Ting, Chen, Ming-Li, & Wang, Jian-Hua. (2018). Supported carbon dots serve as high-performance adsorbent for the retention of trace cadmium. *Talanta (Oxford)*, 180, 18-24.
- Liang Wang, Yanli Wang, Tao Xu, Haobo Liao, Chenjie Yao, Yuan Liu, Minghong Wu. (2014). Gram-scale synthesis of single-crystalline graphene quantum dots with superior optical properties. *Nature Communications*, 5(1), 5357.
- Lim, Shi Ying, Shen, Wei, & Gao, Zhiqiang. (2015). Carbon quantum dots and their applications. *Chemical Society Reviews*, 44(1), 362-381.
- Linehan, K., & Doyle, H. (2014). Efficient one-pot synthesis of highly monodisperse carbon quantum dots. *RSC Advances*, 4(1), 18-21.
- Liu, C., Zhang, P., Zhai, X., Tian, F., Li, W., Yang, J., Liu, Y., Wang, H., Wang, W. and Liu, W. (2012). Nano-carrier for gene delivery and bioimaging based on carbon dots with PEI-passivation enhanced fluorescence. *Biomaterials*, 33(13), 3604-3613.
- Liu, M. L., Chen, B. B., Li, C. M., & Huang, C. Z. (2019). Carbon dots prepared for fluorescence and chemiluminescence sensing. *Science China Chemistry*, 1-14.
- Liu, Mengli, Xu, Yuanhong, Niu, Fushuang, Gooding, J. Justin, & Liu, Jingquan. (2016). Carbon quantum dots directly generated from electrochemical oxidation of graphite electrodes in alkaline alcohols and the applications for specific ferric ion detection and cell imaging. *Analyst (London)*, 141(9), 2657-2664.
- Liu, Q., Guo, B., Rao, Z., Zhang, B., & Gong, J. R. (2013). Strong two-photon-induced fluorescence from photostable, biocompatible nitrogen-doped graphene quantum dots for cellular and deep-tissue imaging. *Nano letters*, 13(6), 2436-2441.
- Liu, R., Wu, D., Liu, S., Koynov, K., Knoll, W., & Li, Q. (2009). An aqueous route to multicolor photoluminescent carbon dots using silica spheres as carriers. *Angewandte Chemie International Edition*, 48(25), 4598-4601.
- Liu, R.; Huang, H.; Li, H.; Liu, Y.; Zhong, J.; Li, Y.; Zhang, S.; Kang, Z. (2014). Metal nanoparticle/carbon quantum dot composite as a photocatalyst for high-efficiency cyclohexane oxidation. *ACS Catal.*, 4, 328–336.
- Liu, Ruili, Wu, Dongqing, Liu, Shuhua, Koynov, Kaloian, Knoll, Wolfgang, & Li, Qin. (2009). An Aqueous Route to Multicolor Photoluminescent Carbon Dots Using Silica Spheres as Carriers. *Angewandte Chemie International Edition*, 48(25), 4598-4601.

- Liu, S., Liu, R., Xing, X., Yang, C., Xu, Y., & Wu, D. (2016). Highly photoluminescent nitrogen-rich carbon dots from melamine and citric acid for the selective detection of iron (III) ion. *RSC advances*, 6(38), 31884-31888.
- Liu, Y., Luo, S., Wu, P., Ma, C., Wu, X., Xu, M., Li, W. and Liu, S. (2019). Hydrothermal synthesis of green fluorescent nitrogen doped carbon dots for the detection of nitrite and multicolor cellular imaging. *Analytica Chimica Acta*, 1090, 133-142.
- Liu, Z., Tabakman, S. M., Chen, Z., & Dai, H. (2009). Preparation of carbon nanotube bioconjugates for biomedical applications. *Nature protocols*, 4(9), 1372-1381.
- Lu, C., Zhang, M., Tang, D., Yan, X., Zhang, Z., Zhou, Z., Song, B., Wang, H., Li, X., Yin, S. and Sepehrpour, H. (2018). Fluorescent metallacage-core supramolecular polymer gel formed by orthogonal metal coordination and host-guest interactions. *Journal of the American Chemical Society*, 140(24), 7674-7680.
- Lu, Jiong., Yang, Jia-Xiang., Wang, Junzhong., Lim, Ailian., Wang, Shuai., & Loh, Kian Ping. (2009). One-pot synthesis of fluorescent carbon nanoribbons, nanoparticles, and graphene by the exfoliation of graphite in ionic liquids. *ACS Nano*, 3(8), 2367-2375.
- Lu, M., Duan, Y., Song, Y., Tan, J., & Zhou, L. (2018). Green preparation of versatile nitrogen-doped carbon quantum dots from watermelon juice for cell imaging, detection of Fe<sup>3+</sup> ions and cysteine, and optical thermometry. *Journal of Molecular Liquids*, 269, 766-774.
- Lu, Yan, Meng, Lianjie, Gao, Yan, Liao, Dongli, Li, Yongxin, Ai, Yongxing, Ma, Yuqin, and Yu, Cong. "A Label Free Ag Sensing Method via in Situ Formation of Metal Coordination Polymer." *Analytical Biochemistry* 549 (2018): 21-25.
- Ma, Z., Ming, H., Huang, H., Liu, Y., & Kang, Z. (2012). One-step ultrasonic synthesis of fluorescent N-doped carbon dots from glucose and their visible-light sensitive photocatalytic ability. *New Journal of Chemistry*, 36(4), 861-864.
- Mao, Xiao-Jiao, Zheng, Hu-Zhi, Long, Yi-Juan, Du, Juan, Hao, Jian-Yu, Wang, Ling-Ling, & Zhou, Dong-Bo. (2010). Study on the fluorescence characteristics of carbon dots. *Spectrochimica Acta. Part A, Molecular and Biomolecular Spectroscopy*, 75(2), 553-557.
- Mehta, A., Mishra, A., Basu, S., Shetti, N. P., Reddy, K. R., Saleh, T. A., & Aminabhavi, T. M. (2019). Band gap tuning and surface modification of carbon dots for sustainable environmental remediation and photocatalytic hydrogen production—A review. *Journal of environmental management*, 250, 109486.

- Miao, X., Qu, D., Yang, D., Nie, B., Zhao, Y., Fan, H., & Sun, Z. (2018). Synthesis of carbon dots with multiple color emission by controlled graphitization and surface functionalization. *Advanced materials*, 30(1), 1704740.
- Mishra, Krishna, Koley, Somnath, & Ghosh, Subhadip. (2019). Ground-State Heterogeneity along with Fluorescent Byproducts Causes Excitation-Dependent Fluorescence and Time-Dependent Spectral Migration in Citric Acid-Derived Carbon Dots. *The Journal of Physical Chemistry Letters*, 10(3), 335-345.
- Mohite, Bhavana V, Koli, Sunil H, & Patil, Satish V. (2018). Heavy Metal. Stress and Its Consequences on Exopolysaccharide (EPS)-Producing *Pantoea* agglomerans. *Applied Biochemistry and Biotechnology*, 186(1), 199-216.
- Molaei, M. J. (2019). A review on nanostructured carbon quantum dots and their applications in biotechnology, sensors, and chemiluminescence. *Talanta*, 196, 456-478.
- Molaei, M. J. (2020). Principles, mechanisms, and application of carbon quantum dots in sensors: a review. *Analytical Methods*, 12(10), 1266-1287.
- Namdari, P., Negahdari, B., & Eatemadi, A. (2017). Synthesis, properties and biomedical applications of carbon-based quantum dots: An updated review. *Biomedicine & Pharmacotherapy*, 87, 209-222.
- Ngah, W.S. Wan, & Fatinathan, S. (2008). Adsorption of Cu (II) ions in aqueous solution using chitosan beads, chitosan–GLA beads and chitosan–alginate beads. *Chemical Engineering Journal (Lausanne, Switzerland: 1996)*, 143(1-3), 62-72.
- Niedz, Randall P, & Evens, Terence J. (2016). Design of experiments (DOE)—history, concepts, and relevance to in vitro culture. In *Vitro Cellular & Developmental Biology. Plant*, 52(6), 547-562.
- Niu, Wen-Jun, Shan, Dan, Zhu, Rong-Hui, Deng, Sheng-Yuan, Cosnier, Serge, & Zhang, Xue-Ji. (2016). Dumbbell-shaped carbon quantum dots/AuNCs nanohybrid as an efficient ratiometric fluorescent probe for sensing cadmium (II) ions and l-ascorbic acid. *Carbon (New York)*, 96, 1034-1042.
- Omidi, M., Yadegari, A., & Tayebi, L. (2017). Wound dressing application of pH-sensitive carbon dots/chitosan hydrogel. *RSC advances*, 7(18), 10638-10649.
- Pal, A., Sk, M., & Chattopadhyay, A. (2016). Conducting Carbon Dot-Polypyrrole Nanocomposite for Sensitive Detection of Picric acid. *ACS Applied Materials & Interfaces*, 8(9), 5758-5762.
- Pan, J., You, M., Chi, C., Dong, Z., Wang, B., Zhu, M., Zhao, W., Song, C., Zheng, Y. and Li, C. (2018). The two dimension carbon quantum dots modified porous g-

- C3N4/TiO<sub>2</sub> nano-heterojunctions for visible light hydrogen production enhancement. *International Journal of Hydrogen Energy*, 43(13), 6586-6593.
- Pan, Lulu, Shan Sun, Aidi Zhang, Kai Jiang, Ling Zhang, Chaoqing Dong, Qing Huang, Aiguo Wu, and Hengwei Lin. (2015). Truly Fluorescent Excitation-Dependent Carbon Dots and Their Applications in Multicolor Cellular Imaging and Multidimensional Sensing. *Advanced Materials*, 27(47), 7782-7787.
- Park, S.Y., Lee, H.U., Lee, Y.C., Choi, S., Cho, D.H., Kim, H.S., Bang, S., Seo, S., Lee, S.C., Won, J. and Son, B.C. (2015). Eco-friendly carbon-nanodot-based fluorescent paints for advanced photocatalytic systems. *Scientific reports*, 5, 12420.
- Peng, J., Gao, W., Gupta, B.K., Liu, Z., Romero-Aburto, R., Ge, L., Song, L., Alemany, L.B., Zhan, X., Gao, G. and Vithayathil, S.A. (2012). Graphene quantum dots derived from carbon fibers. *Nano letters*, 12(2), 844-849.
- Pimpang, P., Sumang, R., & Choopun, S. (2018). Effect of concentration of citric acid on size and optical properties of fluorescence graphene quantum dots prepared by tuning carbonization degree. *Chiang Mai Journal of Science*, 45, 2005-2014.
- Prasad, K., Pallela, R., Kim, D., & Shim, Y. (2013). Microwave-Assisted One-Pot Synthesis of Metal-Free Nitrogen and Phosphorus Dual-Doped Nanocarbon for Electrocatalysis and Cell Imaging. *Particle & Particle Systems Characterization*, 30(6), 557-564.
- Qian, Z., Ma, J., Shan, X., Feng, H., Shao, L. and Chen, J. (2014), Highly Luminescent N-Doped Carbon Quantum Dots as an Effective Multifunctional Fluorescence Sensing Platform. *Chem. Eur. J.*, 20: 2254-2263. doi:10.1002/chem.201304374
- Qu, D., Zheng, M., Zhang, L., Zhao, H., Xie, Z., Jing, X., Haddad, R.E., Fan, H. and Sun, Z. (2014). Formation mechanism and optimization of highly luminescent N-doped graphene quantum dots. *Scientific reports*, 4(1), 1-11.
- Radhakrishnan, K, Sivanesan, S, & Panneerselvam, P. (2020). Turn-On fluorescence sensor based detection of heavy metal ion using carbon dots@graphitic-carbon nitride nanocomposite probe. *Journal of Photochemistry and Photobiology. A, Chemistry.*, 389, 112204.
- Rizzo, C., Arcudi, F., Đorđević, L., Dintcheva, N. T., Noto, R., D'Anna, F., & Prato, M. (2018). Nitrogen-doped carbon nanodots-ionogels: preparation, characterization, and radical scavenging activity. *ACS nano*, 12(2), 1296-1305.

- Ruan, S., Qian, J., Shen, S., Zhu, J., Jiang, X., He, Q., & Gao, H. (2014). A simple one-step method to prepare fluorescent carbon dots and their potential application in non-invasive glioma imaging. *Nanoscale*, 6(17), 10040-10047.
- Sachdev, A., Matai, I., & Gopinath, P. (2016). Carbon dots incorporated polymeric hydrogels as multifunctional platform for imaging and induction of apoptosis in lung cancer cells. *Colloids and Surfaces B: Biointerfaces*, 141, 242-252.
- Sahu, Swagatika, Behera, Birendra, Maiti, Tapas K, & Mohapatra, Sasmita. (2012). Simple one-step synthesis of highly luminescent carbon dots from orange juice: Application as excellent bio-imaging agents Electronic supplementary information (ESI) available. See DOI: 10.1039/c2cc33796g. 48(7), 8835-8837.
- Shan, Xiaoyue, Chai, Lujing, Ma, Juanjuan, Qian, Zhaosheng, Chen, Jianrong, & Feng, Hui. (2014). B-doped carbon quantum dots as a sensitive fluorescence probe for hydrogen peroxide and glucose detection. *Analyst (London)*, 139(10), 2322-2325.
- Shinde, D. B., & Pillai, V. K. (2012). Electrochemical preparation of luminescent graphene quantum dots from multiwalled carbon nanotubes. *Chemistry—A European Journal*, 18(39), 12522-12528.
- Singh, Inderbir, Arora, Riya, Dhiman, Hardik, & Pahwa, Rakesh. (2018). Carbon Quantum Dots: Synthesis, Characterization and Biomedical Applications. *Turkish Journal of Pharmaceutical Sciences*, 15(2), 219-230.
- Song, Y., Zhu, S., Zhang, S., Fu, Y., Wang, L., Zhao, X., & Yang, B. (2015). Investigation from chemical structure to photoluminescent mechanism: A type of carbon dots from the pyrolysis of citric acid and an amine. *Journal of Materials Chemistry C*, 3(23), 5976-5984.
- Sun, C., Zhang, Y., Kalytchuk, S., Wang, Y., Zhang, X., Gao, W., Zhao, J., Cepe, K., Zboril, R., William, W.Y. and Rogach, A.L. (2015). Down-conversion monochromatic light-emitting diodes with the color determined by the active layer thickness and concentration of carbon dots. *Journal of Materials Chemistry C*, 3(26), 6613-6615.
- Sun, Dong., Ban, Rui., Zhang, Peng-Hui., Wu, Ge-Hui., Zhang, Jian-Rong., & Zhu, Jun-Jie. (2013). Hair fiber as a precursor for synthesizing of sulfur- and nitrogen-co-doped carbon dots with tunable luminescence properties. *Carbon*, 64(C), 424-434.
- Sun, Shan, Jiang, Kai, Qian, Sihua, Wang, Yuhui, & Lin, Hengwei. (2017). Applying Carbon Dots-Metal Ions Ensembles as a Multichannel Fluorescent Sensor Array: Detection and Discrimination of Phosphate Anions. *Analytical Chemistry (Washington)*, 89(10), 5542-5548.

- Sun, Ya-Ping, Zhou, Bing, Lin, Yi, Wang, Wei, Fernando, K. A. Shiral, Pathak, Pankaj, Meziani, Mohammed Jaouad, Harruff, Barbara A, Wang, Xin, Wang, Haifang, Luo, Pengju G, Yang, Hua, Kose, Muhammet Erkan, Chen, Bailin, Veca, L. Monica, and Xie, Su-Yuan.(2006). Quantum-Sized Carbon Dots for Bright and Colorful Photoluminescence. *Journal of the American Chemical Society* 128.24: 7756-757.
- Tajik, Somayeh, Dourandish, Zahra, Zhang, Kaiqiang, Beitollahi, Hadi, Le, Quyet Van, Jang, Ho Won, & Shokouhimehr, Mohammadreza. (2020). Carbon and graphene quantum dots: A review on syntheses, characterization, biological and sensing applications for neurotransmitter determination. *RSC Advances*, 1(26), 1546-15429.
- Thete, A. R., Henkel, T., Göckeritz, R., Endlich, M., Köhler, J. M., & Groß, G. A. (2009). A hydrogel based fluorescent micro array used for the characterization of liquid analytes. *Analytica chimica acta*, 633(1), 81-89.
- Tian, J., Leng, Y., Zhao, Z., Xia, Y., Sang, Y., Hao, P., Zhan, J., Li, M. and Liu, H. (2015). Carbon quantum dots/hydrogenated TiO<sub>2</sub> nanobelt heterostructures and their broad spectrum photocatalytic properties under UV, visible, and near-infrared irradiation. *Nano Energy*, 11, 419-427.
- Van der Heide, P., & ProQuest. (2012). X-ray photoelectron spectroscopy an introduction to principles and practices. Hoboken, N.J.: Wiley.
- Wang, Bei-Bei, Jin, Jian-Cheng, Xu, Zi-Qiang, Jiang, Zi-Wen, Li, Xun, Jiang, Feng-Lei, & Liu, Yi. (2019). Single-step synthesis of highly photoluminescent carbon dots for rapid detection of Hg<sup>2+</sup> with excellent sensitivity. *Journal of Colloid and Interface Science*, 551, 101-110.
- Wang, F., Xie, Z., Zhang, H., Liu, C. Y., & Zhang, Y. G. (2011). Highly luminescent organosilane-functionalized carbon dots. *Advanced Functional Materials*, 21(6), 1027-1031.
- Wang, H., Di, J., Sun, Y., Fu, J., Wei, Z., Matsui, H., del C. Alonso, A. and Zhou, S. (2015). Biocompatible PEG-Chitosan@Carbon Dots Hybrid Nanogels for Two-Photon Fluorescence Imaging, Near-Infrared Light/pH Dual-Responsive Drug Carrier, and Synergistic Therapy. *Advanced Functional Materials*, 25(34), 5537-5547.
- Wang, J., Qiu, F., Wu, H., Li, X., Zhang, T., Niu, X., & Xu, J. (2016). A novel water-soluble chitosan linked fluorescent carbon dots and isophorone diisocyanate fluorescent material toward detection of chromium (vi). *Analytical Methods*, 8(48), 8554-8565.



- Wang, R., Lu, K. Q., Tang, Z. R., & Xu, Y. J. (2017). Recent progress in carbon quantum dots: synthesis, properties and applications in photocatalysis. *Journal of Materials Chemistry A*, 5(8), 3717-3734.
- Wang, W., Kim, T., Yan, Z., Zhu, G., Cole, I., Nguyen, N. T., & Li, Q. (2015). Carbon dots functionalized by organosilane with double-sided anchoring for nanomolar Hg<sup>2+</sup> detection. *Journal of Colloid and Interface Science*, 437, 28-34.
- Wang, W., Li, Y., Cheng, L., Cao, Z., & Liu, W. (2013). Water-soluble and phosphorus-containing carbon dots with strong green fluorescence for cell labeling. *Journal of Materials Chemistry B*, 2(1), 46-48.
- Wang, W., Ni, Y., & Xu, Z. (2015). One-step uniformly hybrid carbon quantum dots with high-reactive TiO<sub>2</sub> for photocatalytic application. *Journal of Alloys and Compounds*, 622, 303-308.
- Wang, Wei, Li, Yongmao, Cheng, Lu, Cao, Zhiqiang, & Liu, Wenguang. (2014). Water-soluble and phosphorus-containing carbon dots with strong green fluorescence for cell labeling. *Journal of Materials Chemistry. B, Materials for Biology and Medicine*, 2(1), 46-48.
- Wang, X., Cao, L., Yang, S.T., Lu, F., Mezziani, M.J., Tian, L., Sun, K.W., Bloodgood, M.A. and Sun, Y.P. (2010). Bandgap-Like Strong Fluorescence in Functionalized Carbon Nanoparticles. *Angewandte Chemie*, 122(31), 5438-5442.
- Wang, Y., Myers, M., & Staser, J. (2018). Electrochemical UV Sensor Using Carbon Quantum Dot/Graphene Semiconductor. *Journal of The Electrochemical Society*, 165(4), H3001-H3007.
- Wang, Y., Yang, H., Pschenitzka, M., Niessner, R., Li, Y., Knopp, D., & Deng, A. (2012). Highly sensitive and specific determination of mercury (II) ion in water, food and cosmetic samples with an ELISA based on a novel monoclonal antibody. *Analytical and bioanalytical chemistry*, 403(9), 2519-2528.
- Wang, Yu, Kim, Sung-Hoon, & Feng, Liang. (2015). Highly luminescent N, S- Co-doped carbon dots and their direct use as mercury (II) sensor. *Analytica Chimica Acta*, 890, 134-142.
- Wei, J., Ren, J., Liu, J., Meng, X., Ren, X., Chen, Z., & Tang, F. (2014). An eco-friendly, simple, and sensitive fluorescence biosensor for the detection of choline and acetylcholine based on C-dots and the Fenton reaction. *Biosensors and Bioelectronics*, 52, 304-309.

- Wei, W., Xu, C., Wu, L., Wang, J., Ren, J., & Qu, X. (2014). Non-enzymatic-browning-reaction: a versatile route for production of nitrogen-doped carbon dots with tunable multicolor luminescent display. *Scientific reports*, 4(1), 1-7.
- Weldon, D. G. (2012). THEORY OF INFRARED SPECTROSCOPY.
- Wolfbeis, O. S. (2015). An overview of nanoparticles commonly used in fluorescent bioimaging. *Chemical Society Reviews*, 44(14), 4743-4768.
- Wu, Mingbo, Wang, Yue, Wu, Wenting, Hu, Chao, Wang, Xiuna, Zheng, Jingtang, Li, Zhongtao, Jiang, Bo, and Qiu, Jieshan.(2014). Preparation of Functionalized Water-soluble Photoluminescent Carbon Quantum Dots from Petroleum Coke. *Carbon (New York)* 78: 480-89.
- Wu, Zhu Lian, Zhang, Pu, Gao, Ming Xuan, Liu, Chun Fang, Wang, Wei, Leng, Fei, & Huang, Cheng Zhi. (2013). One-pot hydrothermal synthesis of highly luminescent nitrogen-doped amphoteric carbon dots for bioimaging from Bombyx mori silk - natural proteins. *Journal of Materials Chemistry. B, Materials for Biology and Medicine*, 1(22), 2868-2873.
- Xia, Chunlei, Zhu, Shoujun, Feng, Tanglue, Yang, Mingxi, & Yang, Bai. (2019). Evolution and Synthesis of Carbon Dots: From Carbon Dots to Carbonized Polymer Dots. *Advanced Science*, 6(23), 1901316-N/a.
- Xu, Q., Pu, P., Zhao, J., Dong, C., Gao, C., Chen, Y., Chen, J., Liu, Y. and Zhou, H. (2015). Preparation of highly photoluminescent sulfur-doped carbon dots for Fe (III) detection. *Journal of Materials Chemistry A*, 3(2), 542-546.
- Xu, X. Y., & Yan, B. (2016). Fabrication and application of a ratiometric and colorimetric fluorescent probe for Hg<sup>2+</sup> based on dual-emissive metal–organic framework hybrids with carbon dots and Eu<sup>3+</sup>. *Journal of Materials Chemistry C*, 4(7), 1543-1549.
- Xu, X., Ray, R., Gu, Y., Ploehn, H., Gearheart, L., Raker, K., & Scrivens, W. (2004). Electrophoretic analysis and purification of fluorescent single-walled carbon nanotube fragments. *Journal of the American Chemical Society*, 126(40), 12736-12737.
- Xu, Z.Q., Yang, L.Y., Fan, X.Y., Jin, J.C., Mei, J., Peng, W., Jiang, F.L., Xiao, Q. and Liu, Y. (2014). Low temperature synthesis of highly stable phosphate functionalized two color carbon nanodots and their application in cell imaging. *Carbon*, 66, 351-360.
- Yan, F., Zou, Y., Wang, M., Mu, X., Yang, N., & Chen, L. (2014). Highly photoluminescent carbon dots-based fluorescent chemosensors for sensitive and

- selective detection of mercury ions and application of imaging in living cells. *Sensors & Actuators: B. Chemical*, 192(C), 488-495.
- Yang, G., Wan, X., Su, Y., Zeng, X., & Tang, J. (2016). Acidophilic S-doped carbon quantum dots derived from cellulose fibers and their fluorescence sensing performance for metal ions in an extremely strong acid environment. *Journal of Materials Chemistry A*, 4(33), 12841-12849.
- Yang, Huan, He, Li, Long, Yuwei, Li, Hongxi, Pan, Shuang, Liu, Hui, & Hu, Xiaoli. (2018). Fluorescent carbon dots synthesized by microwave-assisted pyrolysis for chromium (VI) and ascorbic acid sensing and logic gate operation. *Spectrochimica Acta. Part A, Molecular and Biomolecular Spectroscopy*, 205, 12-20.
- Yang, J., Chen, W., Liu, X., Zhang, Y., & Bai, Y. (2017). Hydrothermal synthesis and photoluminescent mechanistic investigation of highly fluorescent nitrogen doped carbon dots from amino acids. *Materials Research Bulletin*, 89, 26-32.
- Yang, Lei., Jiang, Weihua., Qiu, Lipeng., Jiang, Xuwei, Zuo, Daiying, Wang, Dongkai, & Yang, Li. (2015). One pot synthesis of highly luminescent polyethylene glycol anchored carbon dots functionalized with a nuclear localization signal peptide for cell nucleus imaging. *Nanoscale*, 7(14), 6104-6113.
- Yang, Manman, Kong, Weiqian, Li, Hao, Liu, Juan, Huang, Hui, Liu, Yang, & Kang, Zhenhui. (2015). Fluorescent carbon dots for sensitive determination and intracellular imaging of zinc(II) ion. *Microchimica Acta*, 182(15), 2443-2450.
- Yang, S., Sun, J., Li, X., Zhou, W., Wang, Z., He, P., Ding, G., Xie, X., Kang, Z. and Jiang, M. (2014). Large-scale fabrication of heavy doped carbon quantum dots with tunable-photoluminescence and sensitive fluorescence detection. *Journal of Materials Chemistry. A, Materials for Energy and Sustainability*, 2(23), 8660.
- Yang, S.T., Cao, L., Luo, P.G., Lu, F., Wang, X., Wang, H., Meziani, M.J., Liu, Y., Qi, G. and Sun, Y.P. (2009). Carbon dots for optical imaging in vivo. *Journal of the American Chemical Society*, 131(32), 11308-11309.
- Yang, Xingxing, Cui, Fangchao, Ren, Rong, Sun, Jiadi, Ji, Jian, Pi, Fuwei, Zhang, Yinzhi, and Sun, Xiulan. (2019)."Red-Emissive Carbon Dots for "Switch-On" Dual Function Sensing Platform Rapid Detection of Ferric Ions and L-Cysteine in Living Cells." *ACS Omega* 4.7: 12575-2583.
- Yao S, Hu YF, Li GK (2014) A one-step sonoelectrochemical preparation. method of pure blue fluorescent carbon nanoparticles under a high intensity electric field. *Carbon* 66:77–83

- Yu-Fen Wu, Hsi-Chin Wu, Chen-Hsiang Kuan, Chun-Jui Lin, Li-Wen Wang, Chien-Wen Chang, & Tzu-Wei Wang. (2016). Multi-functionalized carbon dots as theranostic nanoagent for gene delivery in lung cancer therapy. *Scientific Reports*, 6(1), 21170.
- Yu, H., Zhao, Y., Zhou, C., Shang, L., Peng, Y., Cao, Y., Wu, L.Z., Tung, C.H. and Zhang, T. (2014). Carbon quantum dots/TiO<sub>2</sub> composites for efficient photocatalytic hydrogen evolution. *Journal of Materials Chemistry A*, 2(10), 3344-3351.
- Yu, H.; Zhang, H.; Huang, H.; Liu, Y.; Li, H.; Ming, H.; Kang, Z. (2012). ZnO/carbon quantum dots nanocomposites: One-step fabrication and superior photocatalytic ability for toxic gas degradation under visible light at room temperature. *New J. Chem.*, 36, 1031–1035.
- Yuan, Y. H., Liu, Z. X., Li, R. S., Zou, H. Y., Lin, M., Liu, H., & Huang, C. Z. (2016). Synthesis of nitrogen-doping carbon dots with different photoluminescence properties by controlling the surface states. *Nanoscale*, 8(12), 6770-6776.
- Yue, J., Li, L., Cao, L., Zan, M., Yang, D., Wang, Z., Chang, Z., Mei, Q., Miao, P. and Dong, W.F. (2019). Two-Step Hydrothermal Preparation of Carbon Dots for Calcium Ion Detection. *ACS Applied Materials & Interfaces*, 11(47), 44566-44572.
- Zeng, J., & Yan, L. (2015). Metal-free transparent luminescent cellulose films. *Cellulose*, 22(1), 729-736.
- Zhai, X., Zhang, P., Liu, C., Bai, T., Li, W., Dai, L., & Liu, W. (2012). Highly luminescent carbon nanodots by microwave-assisted pyrolysis. *Chemical Communications*, 48(64), 7955-7957.
- Zhang, Bing., Liu, Chun-Yan., & Liu, Yun. (2010). A Novel One-Step Approach to Synthesize Fluorescent Carbon Nanoparticles. *European Journal of Inorganic Chemistry*, 2010(28), 4411-4414.
- Zhang, H., Huang, Q., Huang, Y., Li, F., Zhang, W., Wei, C., Chen, J., Dai, P., Huang, L., Huang, Z. and Kang, L. (2014). Graphitic carbon nitride nanosheets doped graphene oxide for electrochemical simultaneous determination of ascorbic acid, dopamine and uric acid. *Electrochimica Acta*, 142, 125-131.
- Zhang, W. J., Liu, S. G., Han, L., Luo, H. Q., & Li, N. B. (2019). A ratiometric fluorescent and colorimetric dual-signal sensing platform based on N-doped carbon dots for selective and sensitive detection of copper (II) and pyrophosphate ion. *Sensors and Actuators B: Chemical*, 283, 215-221.

- Zhang, Y. Q., Ma, D. K., Zhuang, Y., Zhang, X., Chen, W., Hong, L. L., & Huang, S. M. (2012). One-pot synthesis of N-doped carbon dots with tunable luminescence properties. *Journal of Materials Chemistry*, 22(33), 16714-16718.
- Zhang, M., Helleur, R., & Zhang, Y. (2015). Ion-imprinted chitosan gel beads for selective adsorption of Ag<sup>+</sup> from aqueous solutions. *Carbohydrate polymers*, 130, 206-212.
- Zhao, Feiping, Repo, Eveliina, Yin, Dulin, Meng, Yong, Jafari, Shila, & Sillanpää, Mika. (2015). EDTA-Cross-Linked  $\beta$ -Cyclodextrin: An Environmentally Friendly Bifunctional Adsorbent for Simultaneous Adsorption of Metals and Cationic Dyes. *Environmental Science & Technology*, 49(17), 10570-10580.
- Zhou, D., Li, D., Jing, P., Zhai, Y., Shen, D., Qu, S., & Rogach, A. L. (2017). Conquering aggregation-induced solid-state luminescence quenching of carbon dots through a carbon dots-triggered silica gelation process. *Chemistry of Materials*, 29(4), 1779-1787.
- Zhou, Jin, Shan, Xiaoyue, Ma, Juanjuan, Gu, Yamin, Qian, Zhaosheng, Chen, Jianrong, & Feng, Hui. (2014). Facile synthesis of P-doped carbon quantum dots with highly efficient photoluminescence. *RSC Advances*, 4(11), 5465.
- Zhou, T., Ashley, J., Feng, X., & Sun, Y. (2018). Detection of hemoglobin using hybrid molecularly imprinted polymers/carbon quantum dots-based nanobiosensor prepared from surfactant-free Pickering emulsion. *Talanta*, 190, 443-449.
- Zhou, Xu, Zhao, Genfu, Tan, Xiaoping, Qian, Xingcan, Zhang, Ting, Gui, Jingwei, Yang, Long, and Xie, Xiaoguang. (2019). Nitrogen-doped Carbon Dots with High Quantum Yield for Colorimetric and Fluorometric Detection of Ferric Ions and in a Fluorescent Ink. *Mikrochimica Acta* (1966) 186.2: 67.
- Zhou, Y., Sharma, S. K., Peng, Z., & Leblanc, R. M. (2017). Polymers in carbon dots: a review. *Polymers*, 9(2), 67.
- Zhu, C.; Liu, C.; Zhou, Y.; Fu, Y.; Guo, S.; Li, H.; Zhao, S.; Huang, H.; Liu, Y.; Kang, Z. (2017). Carbon dots enhance the stability of CdS for visible-light-driven overall water splitting. *Appl. Catal. B Environ.*, 216, 114–121.
- Zhu, S., Meng, Q., Wang, L., Zhang, J., Song, Y., Jin, H., Zhang, K., Sun, H., Wang, H. and Yang, B. (2013). Highly Photoluminescent Carbon Dots for Multicolor Patterning, Sensors, and Bioimaging. *Angewandte Chemie*, 125(14), 4045-4049.
- Zhu, Shoujun, Zhao, Xiaohuan, Song, Yubin, Lu, Siyu, & Yang, Bai. (2016). Beyond bottom-up carbon nanodots: Citric-acid derived organic molecules. *Nano Today*, 11(2), 128-132.

- Zhuo, Y., Miao, H., Zhong, D., Zhu, S., & Yang, X. (2015). One-step synthesis of high quantum-yield and excitation-independent emission carbon dots for cell imaging. *Materials Letters*, 139, 197-200.
- Zong, J., Zhu, Y., Yang, X., Shen, J., & Li, C. (2010). Synthesis of photoluminescent carbogenic dots using mesoporous silica spheres as nanoreactors. *Chemical Communications*, 47(2), 764-766.
- Zou, F. R., Wang, S. N., Wang, F. F., Liu, D., & Li, Y. (2020). Synthesis of Lanthanide-Functionalized Carbon Quantum Dots for Chemical Sensing and Photocatalytic Application. *Catalysts*, 10(8), 833.
- Zou, S., Hou, C., Fa, H., Zhang, L., Ma, Y., Dong, L., Li, D., Huo, D. and Yang, M. (2017). An efficient fluorescent probe for fluazinam using N, S co-doped carbon dots from L-cysteine. *Sensors and Actuators B: Chemical*, 239, 1033-1041.
- Zuo, P., Xiao, D., Gao, M., Peng, J., Pan, R., Xia, Y., & He, H. (2014). Single-step preparation of fluorescent carbon nanoparticles, and their application as a fluorometric probe for quercetin. *Microchimica Acta*, 181(11-12), 1309-1316.